Thesis for The Degree of Licentiate of Philosophy

Catalyst Interactions and Stability in Polymer Electrolyte Hydrogen Fuel Cells

Nils Rieger

Department of Physics
Chalmers University of Technology
Gothenburg, Sweden, 2026

Catalyst Interactions and Stability in Polymer Electrolyte Hydrogen Fuel Cells

Nils Rieger

Department of Physics
Division of Chemical Physics
Chalmers University of Technology
SE-412 96 Göteborg,
Sweden
Phone: +46(0)31 772 1000

Cover:
Exploded view of a polymer electrolyte fuel cell with a magnified view of the electrode structure (center). An illustration of a quartz crystal (left) and a transmission electron microscope (right) represent the main techniques used in this thesis, namely electrochemical quartz crystal microbalance with dissipation monitoring and identical location transmission electron microscopy.

Printed by Chalmers Digitaltryck,
Gothenburg, Sweden 2026.

"But still try, for who knows what is possible..."
- Michael Faraday

Catalyst Interactions and Stability in Polymer Electrolyte Hydrogen Fuel Cells

Nils Rieger

Department of Physics
Chalmers University of Technology

Abstract

With the progressing climate change and its increasingly tangible impacts, the urgent need for a substantial global reduction in greenhouse gas emissions has become evident. Among the emissions, carbon dioxide is considered the primary driver of climate change, making the decarbonization of high-emission sectors essential. One such sector is transportation, which accounts for significant annual greenhouse gas emissions. Among various approaches to decarbonize transportation, fuel cells operated with hydrogen are regarded as a promising technology, as they emit only water. The high energy density of hydrogen combined with the compact design of fuel cells, particularly polymer electrolyte fuel cells, makes them highly attractive for mobile applications. However, challenges remain, including the reliance on expensive catalyst materials and limited lifetime due to electrode corrosion and catalyst deactivation. Addressing these issues requires both improving efficiency through novel catalysts or optimized utilization and developing strategies to mitigate electrode degradation. Achieving these goals demands a detailed mechanistic understanding of electrode component interactions under dynamic operating conditions.

This thesis investigates ionomer interactions within proton exchange membrane fuel cell (PEMFC) electrodes using electrochemical quartz crystal microbalance with dissipation monitoring (EQCM-D). Measurements on platinum, carbon, and gold electrodes with and without a thin Nafion layer reveal potential-dependent changes in viscoelastic properties linked to ionomer hydration, while being strongly correlated with the oxidation state of the metal/support surface. Similar behavior observed with a spray-coated PEMFC catalyst layer with carbon-supported platinum catalyst during EQCM-D measurements underscores the practical relevance of these findings. Furthermore, the thesis explores degradation suppression in palladium-based anion exchange membrane fuel cell (AEMFC) electrodes via a protective TiO_2-shell, confirmed by identical-location transmission electron microscopy (TEM) imaging and accelerated durability tests. At the same time, enhanced hydrogen oxidation reaction activity is demonstrated for this electrode architecture. Collectively, these studies advance the mechanistic understanding of electrode processes and propose strategies to improve performance and durability of polymer electrolyte hydrogen fuel cells.

Keywords

Fuel cells, Electrochemical quartz crystal microbalance, Ionomer interactions, Identical location electron microscopy, Catalyst degradation

List of Publications

Appended Publications

This thesis is based on the following publications:

I **In-Situ EQCM-D Investigations of PEMFC Catalyst-Ionomer Interactions**,
Nils Rieger, Isak Almyren, Linnéa Strandberg, Martina Butori, Rakel W. Lindström, Björn Eriksson, Patric Jannasch, and Björn Wickman
Accepted, ChemElectroChem.

II **Mechanistic Insight into Hydrogen Oxidation of $Pd@TiO_2$ Core–Shell Catalysts in Alkaline Fuel Cells**,
Benjin Jin, Antti-Jussi Kallio, Nils Rieger, Vasyl Marchuk, Cedric Schiwek, Junjie Shi, Jani Sainio, Hua Jiang, Amine Hammouali, Jefina A S Koivuniemi, Nana Han, Björn Wickman, Simo Huotari, Tanja Kallio
Submitted, under review.

My Contributions

I contributed to the appended publications in the following way:

I I designed and performed all experiments, prepared most of the samples and analyzed the data. For the preparation of some samples I received support from Isak Almyren, Linnéa Strandberg and Martina Butori. I wrote the first draft of the manuscript, which was finalized together with the co-authors.

II I designed and performed the IL-TEM experiments, and analyzed the data for this part of the paper. I wrote the first draft of the corresponding parts in the manuscript.

Contents

Chapter 1

Introduction

Since the dawn of human civilization, the ways in which societies organize themselves have undergone profound transformations. What began as tribal communities struggling for mere survival gradually evolved into complex social structures, where the efficient division of labor enabled new forms of productivity, allowing more and more people to take a break from the constant struggle for survival and thus enjoy a higher standard of living. The pursuit of ever-faster improvements in living standards through process optimization ultimately culminated in industrialization, a turning point that has continued to accelerate technological progress to this day. Over the past two centuries, humanity has witnessed a surge in technological advancement on an unprecedented scale. The age of steam gave way to new propulsion technologies, ultimately ushering in the era of electrification. These developments have revolutionized the areas of food production, transportation, communication and many more. However, a significant consequence of the industrialization era has been the exponential rise in energy demand required to keep the technological instruments of process optimization running. While it took approximately 50 years for energy consumption to double in the early 1800s, by the post-World War II period, starting in 1950, that doubling occurred in just 13.5 years [1, 2]. By 2023, global energy demand had increased to roughly 32 times its level in 1800 [3], with a further yearly rise of 4.3% reported in 2024, according to the IEA Global Energy Review [4].

This dramatic growth has been fueled primarily by the widespread use of fossil energy sources. What began with coal and firewood was soon complemented by oil and natural gas, and to this day, fossil fuels cover the majority of global energy demand [3]. However, their combustion not only releases energy but also generates substantial quantities of CO_2 and waste heat. On the one hand, this means that the energy stored within the energy sources is used very inefficiently. On the other hand, and this has much more serious consequences, increasing energy demand has led to a significant increase in greenhouse gas (GHG) emissions, of which CO_2 is the most prevalent [5]. While the environmental impact of these emissions was negligible during the early stages of industrialization, their cumulative effect has now become alarmingly

evident. As emissions continue to rise almost annually, the global average temperature is also rising steadily, as is the frequency of extreme weather events, posing a direct threat to human life and ecosystems [6]. To mitigate risks, it is absolutely imperative to reduce the total amount of GHGs in the atmosphere, particularly CO_2, or at least halt their continued rise. In general, several different approaches to this problem exist, such as capturing CO_2 directly after it is produced, however, the most straightforward and impactful approach is to reduce reliance on fossil fuels. Since reducing total energy demand seems rather unlikely and insufficient in view of historical developments, the perhaps biggest and most important task for contemporary society is to transition from fossil fuels to renewable energy sources. Solar, wind, and hydroelectric power offer clean alternatives that do not emit GHGs during operation, making them essential components of a sustainable energy future.

As ingenious as the idea of using freely available energy from the sun, wind and water may seem, it nevertheless comes with a number of hurdles which, without appropriate solutions, make it impossible to implement this concept. Even though these energy sources are generally freely available, they are usually not available in the same way at all times. While hydroelectric power is arguably the most consistent renewable energy source, solar and wind power are inherently intermittent, producing little to no energy during periods such as nighttime for solar or calm weather conditions for wind. All these energy sources also entail the generation of very large amounts of energy during peak production. Unfortunately, the timing of peaking energy generation often does not align with consumption patterns. Therefore, with the introduction of energy generation from renewable energy sources, it is essential to also introduce a system for storing surplus energy and releasing it when demand peaks [7].

One solution for implementing this temporary storage is the hydrogen molecule. Long valued as a model system in quantum mechanics, this element is now also viewed as a suitable candidate for large-scale energy storage due to its simplicity. In particular, the fact that 4.48 eV can be stored in the chemical bond between two hydrogen atoms [8] gives the hydrogen molecule this special status. Combined with its low weight, hydrogen boasts the highest gravimetric energy density of any fuel at about $120\,\mathrm{MJ\,kg^{-1}}$, which is about three times that of gasoline [9]. This makes hydrogen particularly interesting for applications that are sensitive to the weight of the energy source, such as aviation, space travel and long-distance transport. In addition, hydrogen can be produced easily by electrolysis of water using surplus electricity, offering a clean and scalable method of energy storage. This is one of the reasons why many political decision-makers are focusing on the development of hydrogen strategies and technologies in order to avert the impending climate crisis, but also to become less dependent on suppliers of fossil fuels, many of which operate under regimes with questionable human rights records. As a result, the so-called hydrogen economy is an integral part of the hydrogen strategy within the European Green Deal adopted by the European Union, which aims to achieve climate neutrality on the European continent by 2050 [10].

A key component of the hydrogen economy includes the efficient recovery

of the energy stored in the chemical bond of hydrogen gas molecules. Fuel cells (FCs), which convert chemical energy directly into electrical energy, are particularly well-suited for this purpose. Unlike conventional combustion-based generators, FCs bypass intermediate conversions, resulting in significantly higher efficiency. When powered by hydrogen derived from renewable sources, FCs emit only water as a by-product, thereby representing a clean, elegant, and sustainable cornerstone for future energy systems.

The concept of FCs is well-developed, and various types exist that differ in both design and operating principles. These differences result in distinct operating conditions, which in turn determine the specific application areas for each FC type. Among them, polymer electrolyte FCs are considered particularly promising candidates for the previously mentioned fields of aerospace and long-distance transport via trucks or ships. This is primarily due to their outstanding efficiency, comparatively low operating temperatures, the use of solid electrolyte materials, and high energy density. These characteristics enable excellent fuel utilization and allow for dynamically adjustable operation thanks to very short activation times, which is an advantage especially relevant in mobile applications.

Despite partial implementation in practice, FC technology has yet to achieve a large-scale breakthrough. The absence of a large-scale breakthrough is due to several factors, with the most significant being the high cost and limited lifetime of these FCs. The high cost is largely driven by the materials used, particularly the catalyst, which typically consists of platinum or other platinum group metals (PGMs). The high material value of these metals prevents a substantial reduction in cost, even with large-scale production [11]. On the other hand, the limited lifetime of FCs is to a large extent attributed to degradation and corrosion of the electrode materials, caused by the harsh reaction conditions during operation. To support competitive commercialization, target parameters were defined several years ago by the U.S. Department of Energy [12]. By 2030, FCs used in heavy-duty vehicles are expected to achieve a cost of \$80 kW^{-1} and a lifetime of 30 000 h. However, these targets are highly ambitious and extremely challenging to meet. Therefore, despite significant performance improvements in recent years, the industry must continue to make substantial efforts to reach these goals. The objective must be to further increase efficiency through electrode design improvements, thereby reducing usage of costly materials, while simultaneously developing strategies to prevent degradation and corrosion. Achieving this requires, first and foremost, a deeper understanding of the processes occurring during FC operation that ultimately lead to performance loss in any form. By identifying these limiting processes, it becomes possible to develop concepts to enhance the stability of FCs.

1.1 Scope of this Thesis

This thesis contributes to the development and refinement of polymer electrolyte-based FCs, thereby advancing this technology toward a GHG-free future. In particular, processes related to the interaction between different electrode components are investigated and analyzed.

To provide the reader with a adequate foundation for discussing the investigations, Chapters 2 and 3 first introduce the fundamental concepts of electrochemistry and catalysis, followed by the basics of hydrogen FCs. Thereafter, Chapter 4 presents a detailed description of the methods used in this work, focusing primarily on electrochemical and physical characterization techniques, including electron microscopy. Finally, Chapter 5 discusses the key findings from **Paper I** and **Paper II**, with a major focus on understanding the interactions between various electrode components during operation, such as catalyst and ionomer. Further parts of this work address strategies to prevent catalyst degradation through the use of protective layers. The thesis concludes by Chapter 6 with a brief summary and recommendations for future research.

Chapter 2

Electrochemistry & Catalysis

To gain a comprehensive understanding of hydrogen FCs it is necessary to explore the fundamental principles and concepts involved. These include, first, electrochemistry, as FCs rely on electrochemical processes to generate electric current. Second, the concept of catalysis must be considered, since without the use of catalysts, the practical efficiency of FCs would be severely limited. Ultimately, both concepts are closely intertwined in the context of FCs, where they are applied simultaneously. As such, they must be considered in combination, an exploration that is addressed in the section on catalysis in electrochemical systems.

2.1 Electrochemistry

Electrochemistry is a subfield of chemistry and, as the name suggests, deals with the relationship between electrical energy and chemical reactions. The fact that these two phenomena are connected is, however, not immediately intuitive. One of the earliest discoveries in this area dates back to the Italian scientist Luigi Galvani, who in 1786 observed that the legs of a dead frog twitched when touched with two metal pieces connected in an electrical circuit. Galvani then mistakenly attributed this effect to what he called "animal electricity" [13]. It was Alessandro Volta who later clarified that the electricity was generated by the contact between two different metals via the muscle tissue. Based on this insight, Volta constructed the "voltaic pile", which went down in history as the first practical battery [14, 15].

This invention can be considered the birth of electrochemistry, as it demonstrated a clear link between chemical reactions and electrical energy. It not only transformed our understanding of chemical processes but also had a profound impact on everyday life. In today's world, batteries of all kinds are indispensable, since without the ability to store electrical energy in chemical form, countless devices such as mobile phones, laptops, and other technical

equipment would be unusable. Building on the same principles, it was later found that the controlled application of electrical potentials and currents enables the production of materials with high purity and precision, as seen in electroplating or hydrogen production via electrolysis.

The Electrochemical Setup

To understand the foundations of electrochemistry, it is instructive to begin with the early experiments of Galvani and Volta. In both cases, it was observed that an electric current was generated when two pieces of metal came into contact with an ion-containing solution. In the case of the Voltaic pile, the metals used were zinc and copper plates, separated by cloth soaked in brine [15]. When both plates were connected via an electrical circuit, an electric current began to flow through the circuit. The occurrence of this current implies the existence of a potential difference between the two metal plates, causing electrons to move from one metal to the other. This, in turn, means that electrons are released at one electrode and consumed at the other, participating in electrochemical reactions occurring at the surfaces of the metal plates. In the case of the Voltaic pile, the following reactions take place:

$$\mathrm{Zn} \longrightarrow 2\,\mathrm{e}^- + \mathrm{Zn}^{2+} \tag{2.1}$$

$$\mathrm{Cu}^{2+} + 2\,\mathrm{e}^- \longrightarrow \mathrm{Cu} \tag{2.2}$$

Thus, two distinct reactions occur, one at the zinc plate (equation 2.1) and one at the copper plate (equation 2.2). The zinc plate begins to dissolve, releasing electrons, while the natural oxide layer on the copper plate is gradually transformed to elemental copper as electrons are added. This reaction proceeds spontaneously until the oxide layer on the copper surface is fully consumed. This setup illustrates several general principles that apply to electrochemical systems. Typically, such systems consist of two or more electrodes that are electrically connected, usually via an external circuit. In this case, the zinc and copper plates serve as the electrodes, with zinc acting as the anode and copper as the cathode. Another essential component is an ion-conducting medium that separates the electrodes while being insulating to electrons. Often, this medium is an aqueous electrolyte solution, such as the brine in the Voltaic pile, though other media, such as ion-conducting membranes, are also possible. This electrolyte enables ionic mobility, allowing for charge compensation, and at the same time spatial separation of the reactions occurring at the respective electrodes, the so-called half-reactions. In any electrochemical setup, these half-reactions occur in pairs: one oxidation and one reduction. In the present case, equation 2.1 represents the oxidation reaction, and equation 2.2 the corresponding reduction. Together, they form the overall redox reaction, which constitutes the fundamental basis of all electrochemical processes [16]. A general schematic of such an electrochemical setup is shown in Figure 2.1.

It is important to note that the half-reactions in a redox process are, in principle, interchangeable, and the electrode itself does not necessarily

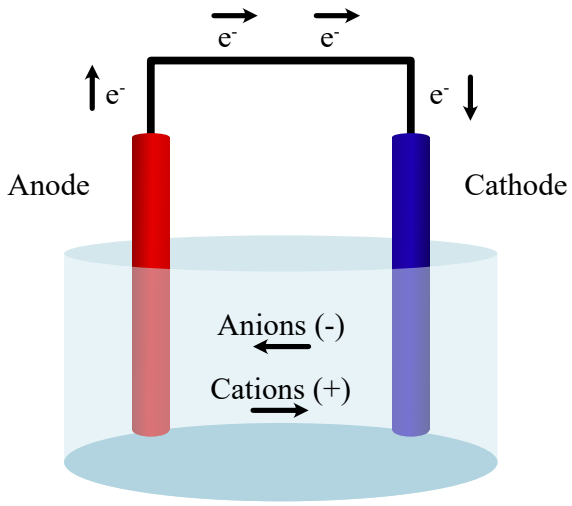

Figure 2.1: Simplified schematic of a general electrochemical setup. Two electrodes, anode and cathode, are connected via an electrical circuit, which allows for the flow of an electrical current. During the reaction, anions and cations present in the electrolyte solution move towards the anode and cathode, respectively.

participate directly in the chemical reaction. In the Voltaic pile, for example, once the copper oxide layer is consumed, a different reaction begins at the cathode, where hydronium ions present in the brine are reduced to elemental hydrogen:

$$2\,H_3O^+ + 2\,e^- \longrightarrow H_2 + 2\,H_2O \tag{2.3}$$

At this point, the copper electrode is no longer directly involved in the reaction, but only offers a surface for this reaction to occur. The fact that redox reactions can occur at electrode surfaces, where the electrode merely serves as an electron donor or acceptor, will be highly relevant throughout this thesis.

However, not all combinations for redox reactions occur spontaneously. For example, in the electrolysis of water, where water molecules are split into elemental hydrogen and oxygen, simply placing two electrodes in an aqueous solution is insufficient to initiate the reaction. To drive this process, more than just electrical contact is required. Instead, a voltage must be applied across the electrodes. To understand why this is necessary requires a deeper examination of the fundamental physical and chemical principles, specifically, the thermodynamic basics of electrochemistry.

Thermodynamical Basics

Electrochemistry is of course subject to the laws of thermodynamics, which provide the framework for explaining and understanding electrochemical behavior. As such, redox reactions, similar to acid-base reactions, are generally equilibrium reactions, and in their simplest form, they can be described in the

following way [17]

$$\mathrm{Ox} + n\mathrm{e}^- \rightleftharpoons \mathrm{Red} \tag{2.4}$$

Here, the oxidized species Ox transfers a number of n electrons to the reduced species Red. For equilibrium reactions of this type, the change in Gibbs free energy ΔG can be expressed as [18]

$$\Delta G = \Delta H - T\Delta S = \Delta G^0 + RT \ln Q_r \tag{2.5}$$

In this context, R and T represent the gas constant and the absolute temperature, respectively. ΔG^0 denotes the change in Gibbs free energy under standard conditions, and Q_r is the reaction quotient, which describes the ratio of the activity of the reduced species to that of the oxidized species. It is the change in Gibbs free energy, ΔG, that ultimately determines whether a reaction proceeds spontaneously or not. If $\Delta G < 0$, the reaction occurs spontaneously, and the system is classified as a galvanic cell in electrochemical terms. Conversely, if $\Delta G > 0$, the reaction is non-spontaneous and requires external energy input, making it an electrolytic cell. Hereby, ΔG corresponds either to the maximum amount of work the system can perform (in a galvanic cell), or to the minimum amount of work that must be supplied to the system to drive the reaction (in an electrolytic cell). Since we are dealing with electrochemical systems, this work is specifically electrical work, which is defined as

$$W_{max} = \Delta G = W_{electrical} = -nFE_{cell} \tag{2.6}$$

Thus, both the electrical work $W_{electrical}$ and, consequently, the change in Gibbs free energy are directly related to the cell potential E_{cell}, whereby F is the Faraday constant and n the number of moles of electrons transferred [17]. This also implies that the Gibbs free energy is directly influenced by the cell potential. In other words, the thermodynamic energy landscape can be altered by injecting electrical energy in such a way that a reaction, which is non-spontaneous under standard conditions, can occur simply by application of a suitable potential. Electrochemistry, thus, enables reactions that would not proceed without this electrical energy input. This is ultimately the reason why water can be split via electrolysis and why batteries can be charged by connecting them to a power source. The theoretically maximum potential that a galvanic cell can deliver (or the minimum potential that must be applied to drive an electrolytic cell) is directly determined by the Gibbs free energy of the corresponding reaction. Furthermore, this relation between electrical work and the Gibbs free energy can be used to derive an expression for the cell potential in an equilibrium state by combining equations 2.5 and 2.6 as follows:

$$-nFE_{cell} = -nFE^0_{cell} + RT \ln Q_r \tag{2.7}$$

which can be converted into the form of the Nernst equation by dividing by $-nF$:

$$E_{cell} = E^0_{cell} - \frac{RT}{nF} \ln Q_r \tag{2.8}$$

This equation forms the core of electrochemistry, as it allows for a relationship between the electrical quantity of potential and chemical quantity concentration in the form of activity within the reaction quotient Q_r. It is valid in this form for redox reactions of any complexity, since Q_r can be expressed either as the reaction quotient of the half-cell reaction according to equation 2.4 or as the ratio of the reaction quotients of all reactions at the electrodes of a cell [17]. In the latter case, the cell potential under equilibrium conditions E^0_{cell} can be derived from the standard half-cell potentials in the following way:

$$E^0_{cell} = E^0_{red} - E^0_{ox} \tag{2.9}$$

In general, the Nernst equation describes the cell potential of an electrochemical system as a function of concentration. At equilibrium, the rates of the forward and reverse reactions are equal. This does not imply that the reactions cease to occur, but rather that they proceed in such a way that their net effect cancels out. Consequently, the system is said to be in a state of dynamic equilibrium. In the context of electrochemical reactions, this means that no net current flows between anode and cathode. However, when the system is perturbed, for example by the introduction of concentration gradients, the balance between the forward and reverse reactions is disrupted. One reaction proceeds at a higher rate than the other, resulting in a net current. According to the Nernst equation, this shift away from equilibrium is accompanied by a deviation of the cell potential from its equilibrium value.

Such deviations are ubiquitous in real electrochemical systems. For instance, the voltage measured during the operation of a FC rarely matches the nominal standard cell potential. The difference between the measured potential and the thermodynamically determined equilibrium potential is referred to as the overpotential, defined as:

$$\eta = E - E^0_{cell} \tag{2.10}$$

In practice, this overpotential can either increase or decrease the observed cell voltage in relation to the thermodynamically determined equilibrium potential, depending on the type of electrochemical cell. In galvanic cells, the overpotential results in a decrease in the measured cell voltage, meaning that less energy can be extracted from the system than theoretically possible. Conversely, in electrolytic cells, the overpotential leads to an increase in the required voltage, implying that surplus energy must be supplied to drive the reaction. In both cases, the excess energy associated with the overpotential is primarily dissipated as heat and is therefore not available for useful work. The specific causes of these losses can vary and will be discussed in detail in a later chapter, when the operational principles of FCs are examined. However, first, it is important to address how this overpotential influences the kinetics of the electrochemical reactions involved.

Overpotential and Reaction Kinetics

The consideration of reaction kinetics is particularly important at this stage, as it allows the behavior of the observed current density to be described as a function of the overpotential. This can be achieved by relating Faraday's law, which connects reaction rate to current density, to the Gibbs free energy of the kinetically limiting transition states. Although a detailed derivation is not provided here, the assumption that the reactions are kinetically limited by charge transfer rather than mass transport yields the so-called Butler-Volmer equation in the form of [16]:

$$j = j_{ox} - j_{red} = j_0 \left(e^{\frac{(1-\alpha)nF\eta}{RT}} - e^{\frac{-\alpha nF\eta}{RT}} \right) \tag{2.11}$$

This equation shows that the total current density j is composed of the partial current densities resulting from oxidation and reduction, j_{ox} and j_{red}, respectively. These anodic and cathodic contributions scale exponentially with the overpotential η, where the slope of the exponential dependence is governed by the charge transfer coefficient α and the number of electrons transferred n. The pre-exponential factor j_0, known as the exchange current density, has a particularly significant influence on the total current density. In practice, it determines how much overpotential is required to achieve high current densities and, consequently, fast reaction kinetics. This observation is crucial to the chapter on catalysis in electrochemical systems and should therefore be kept in mind for a deeper understanding.

By taking a closer look at equation 2.11 two limiting cases of the Butler-Volmer equation can be identified. In the case of very small overpotentials ($\eta < 10\,\mathrm{mV}$), the exponents within the equation have low enough values for the exponential functions to be approximated by a power series. Neglecting the terms of the second order or higher results in a linear dependence of the current density on the potential. Consequently, in accordance with Ohm's law, the charge transfer resistance R_{ct} can be determined from this dependence, which in turn allows for inferences regarding j_0. The current density can therefore be approximated for small overpotentials by:

$$j \approx j_0 \frac{nF}{RT}\eta = R_{ct}\eta \tag{2.12}$$

In the case of high overpotentials, the total current density is dominated by only one of the two partial current densities, while the other partial current density approaches zero. Accordingly, for sufficiently negative overpotentials, $j \approx j_{ox}$ and, conversely, for sufficiently positive overpotentials, $j \approx j_{red}$. Thus, for the corresponding cases, this results in simplified expressions of the form of

$$j \approx j_0 e^{\frac{-\alpha nF\eta}{RT}} \qquad \eta \ll 0 \tag{2.13}$$

$$j \approx j_0 e^{\frac{(1-\alpha)nF\eta}{RT}} \qquad \eta \gg 0 \tag{2.14}$$

The handling of these equations becomes more intuitive when expressed in logarithmic form. This representation enhances interpretability, as the logarithm of the current density exhibits a linear dependence on the overpotential.

The slope of these linear regions of the Butler–Volmer equation is commonly referred to as the Tafel slope [16, 19]. A graphical illustration of this relationship is shown in Figure 2.2, and the corresponding logarithmic expressions for the current density at cathodic and anodic overpotentials can be written as follows:

$$\log j = \log j_0 - \frac{\alpha n F}{2.303 R T}\eta \qquad \eta \ll 0 \tag{2.15}$$

$$\log j = \log j_0 + \frac{(1-\alpha) n F}{2.303 R T}\eta \qquad \eta \gg 0 \tag{2.16}$$

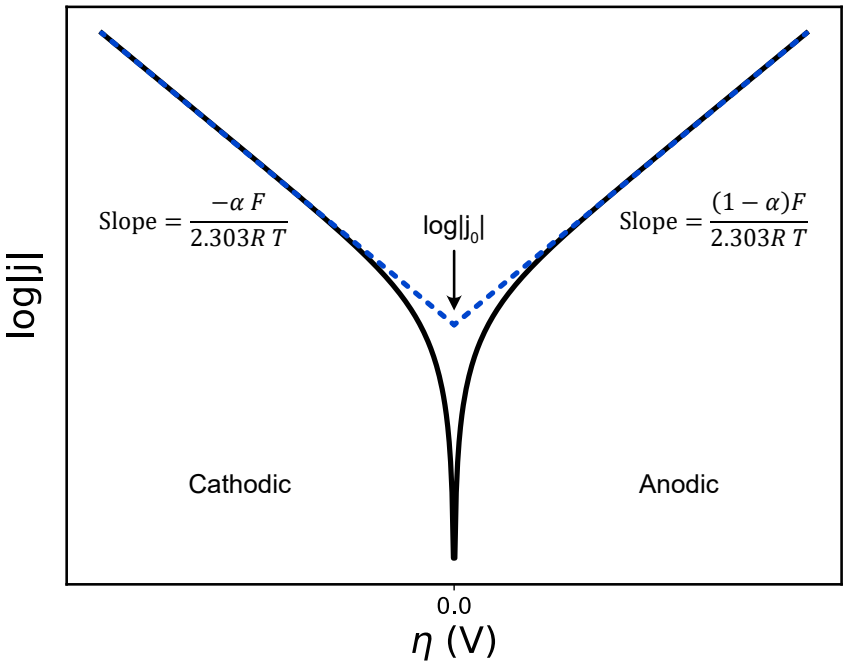

Figure 2.2: Visualization of the logarithmic form of the Butler-Volmer equation, with the dashed lines indicating the Tafel slopes for the cathodic and anodic limiting case.

Reference Potentials

Before we can address how kinetic processes can be improved in general, one final concept must be discussed, namely the definition of the electrode potential in electrochemical redox reactions. While the electrode potential is generally related to the Gibbs free energy, as previously discussed, determining the absolute, true electrode potential is practically impossible. To still be able to classify and compare the electrode potential of a given electrochemical reaction, a reference system is typically used. This reference is usually a reference electrode, and what is measured is the potential difference between two electrodes. This potential difference can, in turn, be related to the change in Gibbs free energy. By introducing such a reference system, it becomes possible to compare and categorize the electrode potentials of different redox

reactions. To simplify this classification, the IUPAC has defined the so-called standard hydrogen electrode (SHE) as a universal reference point [20]. Electrode potentials are therefore typically reported as standard reduction potentials relative to the SHE, which is assigned a standard electrode potential of 0 V. The corresponding redox pair the SHE refers to is defined as:

$$2\,H^+ + 2\,e^- \rightleftharpoons H_2 \tag{2.17}$$

This equation describes a similar reaction as equation 2.3. It is important to note, however, that the redox reaction takes place on a platinized platinum surface, as platinum is an exceptionally inert metal with a very high intrinsic exchange current density with respect to this reaction. The platinum electrode is immersed in an acidic solution with a proton concentration of $1\,\mathrm{mol\,L^{-1}}$ and a hydrogen pressure of 1 bar. Unfortunately, using the SHE as a universal reference is challenging because electrolytes rarely match this defined proton concentration due to variations in pH between different electrolytes. This makes the SHE impractical for many applications. To overcome this limitation, the reversible hydrogen electrode (RHE) is commonly used instead. The RHE is based on the same redox pair as shown in equation 2.17, but it can operate in electrolytes of any pH. Its potential shifts with pH (approximately 59 mV per pH unit at room temperature), yet this predictable variation makes the RHE a convenient and versatile reference electrode for in-situ measurements.

2.2 Catalysis

As described in the previous section, electrochemical reactions are redox reactions and, in general, equilibrium reactions. When such a reaction is at equilibrium, the rate of the forward and backward reactions is equal, meaning that the same amount of reactants is converted into products as vice versa. Generally speaking, an equilibrium reaction can be expressed as follows:

$$A + B \rightleftharpoons AB \tag{2.18}$$

In applications like FCs, however, a balanced state is not desirable, as the goal is to generate current from a reaction. In that specific case the forward reaction is to be favored, so the equilibrium must be shifted in that direction. In electrochemical systems, that can be achieved by introducing a potential difference between the two electrodes. But in practice, it is not only important whether a reaction can occur at all. If a reaction is thermodynamically preferred, it is for practical reasons important to have a rate that is fast enough, as this is what directly determines the amount of current that can be generated by the FC. The rate of a reaction describes the speed of a reaction and, for a first order reaction, can be expressed as:

$$r = kC \tag{2.19}$$

This equation states that the reaction rate r depends on the concentration of the reactants C [21]. The simplest way to increase the reaction rate is

therefore to significantly raise the concentration of the reactants relative to the products. The rate depends also on the rate constant k. This constant itself incorporates several influencing factors and is phenomenologically described by the Arrhenius equation: [22]

$$k = Ae^{-\frac{E_a}{RT}} \tag{2.20}$$

In this equation, A represents the pre-exponential factor, R is the ideal gas constant, and T is the absolute temperature of the system. The latter, in particular, is an important parameter for influencing the reaction rate, but in real systems, increasing temperature often comes at the cost of efficiency, since generating heat requires energy input. This leaves the final factor, the activation energy E_a, as the most effective lever for improving reaction rates. Activation energy describes the energy barrier that must be overcome for a reaction to proceed. Even if the difference in Gibbs free energy ΔG is negative (indicating a spontaneous reaction), the energy barrier between different energetic states occurring during the reaction ultimately determines the reaction rate.

This is precisely where the concept of catalysis comes into play. A catalyst, by definition, increases the reaction rate by providing reaction paths with lower activation energy without being consumed in the process. In general, there exist several fundamental principles of catalysis, which can be outlined as follows [21]:

1. A catalyst lowers the activation energy of a reaction by providing an alternative reaction pathway with a lower overall energy barrier.

2. Despite the reduced activation energy, the overall change in energy, specifically the Gibbs free energy, remains unchanged by the use of a catalyst. This means that a catalyst has no influence on the equilibrium of a reaction, as it only affects kinetics, not thermodynamics. As a consequence, a catalyst always accelerates both the forward and backward reaction.

3. A catalyst provides specific sites where reactants can adsorb, meet, and be brought into close proximity. In this way, the catalyst effectively assembles the reactants to facilitate the reaction.

The impact of these three fundamental principles on the reaction pathway of the reaction described in equation 2.18 is illustrated schematically in Figure 2.3. In this diagram, the catalyst provides a surface for reactants A and B to adsorb. Once adsorbed, the reactants can interact more easily due to their binding to the catalyst, which lowers the energy required for the reaction, reflected in the reduced activation energy. After the product AB is formed, it can desorb from the catalyst surface. Although this catalyzed reaction pathway is more complex than the uncatalyzed one, the overall energy barrier that must be overcome to form the product AB is significantly lower. It should be noted that the mechanism described here refers specifically to heterogeneous catalysis.

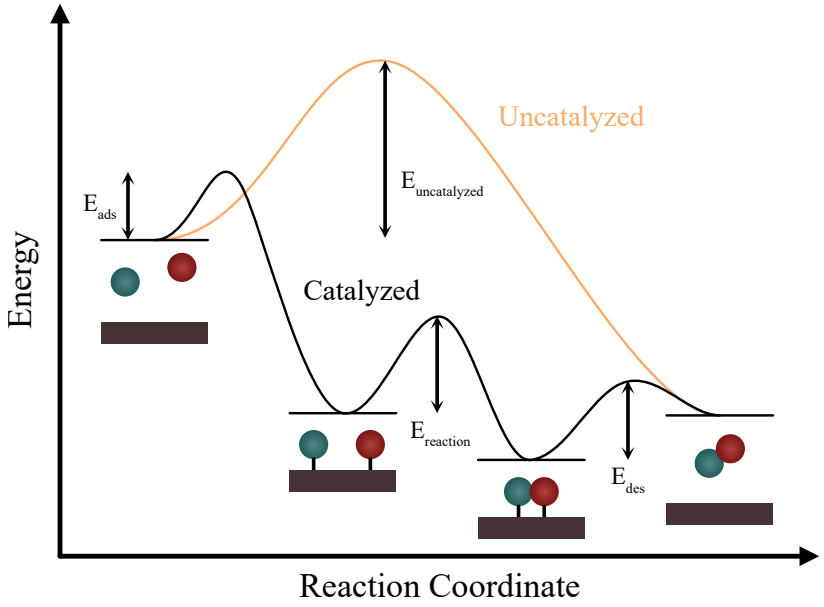

Figure 2.3: Generic energy diagram of a chemical reaction. The uncatalyzed reaction path has a high energy barrier, while the catalyst offers a reaction path with lower energy barriers.

Generally, there are two main types of catalysis: homogeneous and heterogeneous. Homogeneous catalysis occurs when the catalyst and reactants are in the same phase, which typically is in liquid or gas form, and is common in enzymatic systems, for example. In FCs, and therefore in the context of this thesis, only heterogeneous catalysis is relevant, where the catalyst is in a different phase than the reactants. In practice, this means that the catalyst in FCs is solid, while the reactants are either liquid or gaseous. Accordingly, the following chapters will focus exclusively on heterogeneous catalysis.

In addition to illustrating the reaction path, Figure 2.3 also allows for a derivation of the fundamental requirements for a catalyst. Since the catalyzed path is generally more complex and involves multiple intermediate steps, each of these steps is associated with its own energy barrier. Hence, this reaction path includes an energy barrier for the adsorption of reactants A and B, as well as an energy barrier for the desorption of the product AB. These energies depend on the specific catalyst material and the reactants involved. Intuitively, it becomes clear that both excessively strong and excessively weak binding of the reactants to the catalyst surface can hinder the overall reaction. In general, the requirements for a suitable catalyst can be described as follows [21]:

- The reactants A and B should not bind too weakly to the catalyst surface, as the reaction pathway shown would otherwise not be accessible.

- Both reactants should exhibit similar and moderate affinity for adsorption on the catalyst surface. Otherwise, the surface may become overly populated by one species, limiting the availability of active sites, meaning those sites that are essential for the catalytic process.

- The product AB should bind as weakly as possible to the surface to promote desorption. This, as well, prevents the blocking of active sites on the catalyst surface.

These requirements were summarized by Paul Sabatier in what is now known as the Sabatier principle [23]. This qualitative concept states that there is a "sweet spot" in catalyst selection, where reactants bind neither too strongly nor too weakly to the surface [24]. The Sabatier principle is commonly visualized using the volcano plot, in which the catalytic activity of various catalyst materials is plotted against the binding energy of the reactants to the surface. The resulting distribution resembles the shape of a volcano, with the peak representing the optimal binding strength where the catalyst exhibits the highest activity. A schematic representation of this concept is shown in Figure 2.4.

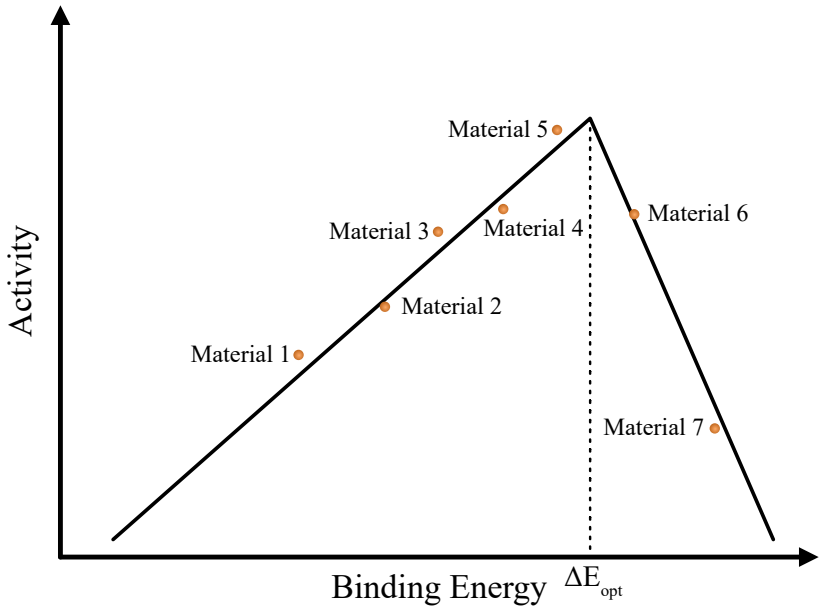

Figure 2.4: Generic volcano plot for an arbitrary reaction as a visualization of Sabatier's principle. Different materials possess different binding energies to the reactants and therefore different activity as a catalyst for the reaction. ΔE_{opt} indicates the optimal binding energy.

Activity alone, however, is not sufficient to determine whether a material is a suitable catalyst for a given reaction. While this parameter is fundamentally important, other factors such as selectivity and stability also influence catalyst selection. In particular, the selectivity of a catalyst determines whether efficient catalysis of a reaction is possible. Selectivity describes whether a given catalyst material can produce the desired reaction product preferentially, ideally without generating any by-products. By-products may occur, for example, when a reaction can proceed via multiple pathways or when additional species are present during the reaction. In such cases, the catalyst must favor the desired pathway, thereby ensuring a high ratio of product to by-products. High selectivity can often be achieved through preferential adsorption of certain

species on the catalyst surface, but other approaches exist as well, such as tailoring the catalyst's morphology or introducing steric hindrance to suppress the formation of undesired products.

2.3 Catalysis in Electrochemical Systems

In principle, catalysis in electrochemical systems follows the same rules as outlined previously. There are, nevertheless, several important distinctions to consider. In conventional catalytic systems, a catalyst provides an energetically favorable reaction pathway by allowing reactants to adsorb onto its surface. Electrochemical reactions are fundamentally different due to the spatial separation of the oxidation and reduction half-reactions. Each half-reaction is catalyzed independently by its respective catalyst and electric charge must be able to flow between them. This means that a catalyst in an electrochemical system must be capable of facilitating the transfer of the electrical charge involved in the half-reaction it supports. Thus, the ability of a catalyst to efficiently mediate charge transfer between its surface and the reactants is a critical factor in its performance. Accordingly, the catalyst in electrocatalysis often serves either directly as the electrode, such as the copper electrode in the voltaic pile described in equation 2.3, or is dispersed on the electrode surface. In general, several key factors can be defined that determine the performance of a catalyst:

- **Activity**: A measure of the effective rate at which a catalyst facilitates a specific reaction under given conditions. In electrochemical systems, following Faraday's law, this rate is typically expressed in terms of current density.
- **Selectivity**: The ability of a catalyst to preferentially promote the formation of a specific desired product over other possible products.
- **Stability**: The ability of the catalyst to resist degradation and corrosion under harsh (electro)chemical conditions.

In applications such as FCs, the current density, which is a measure of activity, is often the most critical parameter for evaluating catalyst performance. As discussed in Chapter 2.1, the exchange current density acts as an multiplicative term in the expression for current density (equation 2.11) and thus strongly influences reaction kinetics. It is a material dependent parameter and determines how much overpotential is required to achieve a given current density and thus a given reaction rate. In that way, the current density is commonly used as a measure for the performance of a catalyst and if a Material 1 can achieve a higher current density than Material 2 at the same overpotential, then Material 1 is considered to have a higher activity for that reaction. However, it is important to note that catalysis is highly surface-sensitive, and a larger electrochemically active surface area (ECSA) generally leads to higher current densities. For this reason, current densities are typically normalized to either the ECSA or the mass of the catalyst resulting in measures for the

specific or mass activity, respectively, to allow for meaningful comparisons between different materials. Once a catalyst with satisfactory activity has been identified, the other two factors, selectivity and stability, must also be considered to optimize its performance in a given practical application.

Chapter 3

Hydrogen Fuel Cells

After discussing the key thermodynamic and kinetic principles in the previous chapter, the following chapter can now address the main subject of this thesis: the fuel cell (FC). In general, a FC can be described as an electrochemical cell that provides direct access to the energy released during an electrochemical reaction. While the specific reaction taking place is interchangeable, the FC itself essentially provides a framework that allows the reaction to proceed in a controlled manner. This enables the direct conversion of chemical energy into electrical energy. This direct conversion is achieved by spatially separating the two half-reactions of the redox process. Crucially, this separation must be both physically and electrically insulating so that the electrons transferred in the redox reaction cannot take the direct path between the two reaction sites. Instead, they are forced to flow through an external electrical circuit, where the resulting current can perform useful work. This principle forms the core idea behind the concept of a FC and applies universally.

In practical implementations, however, FCs differ in many aspects, most notably in the type of fuel used. In principle, any fuel capable of releasing energy through an oxidation reaction can be employed, including light hydrocarbons. Nevertheless, the most important fuel in the context of FCs and particularly relevant for zero-emission energy systems is hydrogen. In fact, the first FC ever conceptualized, by Sir William Grove in 1838, was a hydrogen FC [25]. Later, this technology gained prominence through its use in NASA space missions and has since been continuously developed and improved. Today, in the pursuit of emission-free energy systems, hydrogen FCs are more relevant than ever.

3.1 Hydrogen as an Energy Carrier

The current relevance of hydrogen FCs is not solely due to the technology itself. Rather, as described in the Introduction (Chapter 1), hydrogen FCs represent just one component of a broader, integrated system aimed at replacing fossil energy carriers with alternative energy storage methods in the long term. At the center of this concept is hydrogen, envisioned as an energy carrier. The approach is based on the expansion of renewable energy sources such as

solar, wind, and hydropower, and the principle that surplus energy from these sources under favorable conditions is used to produce hydrogen. The preferred method for hydrogen production is water electrolysis, as it is relatively simple to implement and can often be carried out directly on-site. This technology, much like FCs themselves, has been known for a long time, dating back to the early 1800s when William Nicholson and Anthony Carlisle first performed water electrolysis using the previously introduced voltaic pile [26]. Later, starting around 1930, water electrolysis was adopted on an industrial scale for large-scale hydrogen production. When this process is powered by renewable energy, the resulting hydrogen is referred to as green hydrogen, meaning hydrogen with a minimal greenhouse gas footprint. In this way, surplus electrical energy from zero-emission sources can be stored as chemical energy in hydrogen gas. This stored energy can thereafter be kept for extended periods and delivered to consumers as needed. Hydrogen can serve two primary purposes: On the one hand, hydrogen can be used to feed electricity directly into the grid, for example when electricity from renewable energies is only available to a limited extent due to unfavorable conditions. In this case, hydrogen can be used to compensate for major imbalances in energy production, such as seasonal fluctuations. On the other hand, hydrogen offers the unique potential to act as a fuel and feedstock across both mobile and industrial applications. This versatility forms the foundation of the hydrogen economy, as illustrated in Figure 3.1.

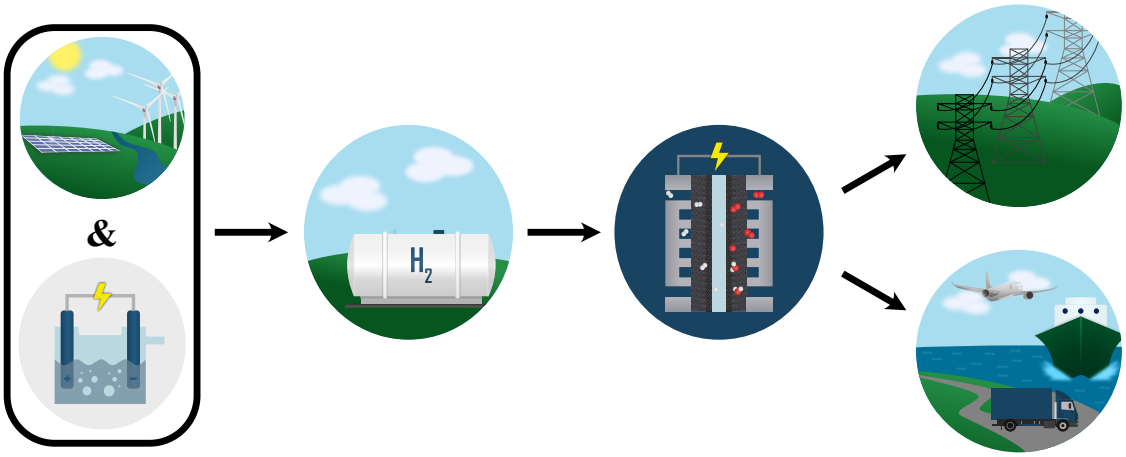

Figure 3.1: Schematic illustration of the hydrogen economy with the fuel cell as a centerpiece connecting energy storage and consumers.

Mobile applications primarily include sectors such as road, rail, maritime, and air transport. Collectively, the transportation sector accounted for approximately 17.9% of global greenhouse gas emissions in 2022 [27], with a rising trend. Decarbonizing this sector therefore offers enormous potential for emission reductions. Hydrogen can play a key role here, particularly in cases where battery-based electrification is not feasible. While batteries store and deliver energy with higher efficiency, their gravimetric energy density (typically $0.1\,\mathrm{MJ\,kg^{-1}}$ to $2\,\mathrm{MJ\,kg^{-1}}$) is significantly lower than that of conventional fuels [28, 29]. Hydrogen, by contrast, offers a much higher gravimetric energy density,

making it an attractive option for applications requiring long ranges or where weight is critical. Consequently, hydrogen is considered a suitable fuel for long-haul trucks, ships, and potentially even aircraft. At the center of all these applications within the hydrogen economy lies the FC, the key device for efficiently converting chemical energy into electrical energy. To understand how this conversion occurs, which half-reactions are involved and must be controlled, and how efficiency can be improved through targeted design, it is essential to first examine the fundamental concept and underlying principles of FCs in detail.

3.2 The Concept Behind Fuel Cells

In hydrogen-based FCs, the primary objective is to oxidize the fuel using an oxidizing agent. Typically, oxygen from the ambient air serves as the oxidant. The overall redox reaction for a hydrogen FC is given by:

$$2\,H_2 + O_2 \longrightarrow 2\,H_2O \tag{3.1}$$

Under standard conditions, this reaction is highly exothermic, producing water and releasing energy. To efficiently convert this energy into electrical power, the underlying redox process is split into two half-reactions that occur at physically separated electrodes within the FC. The hydrogen oxidation reaction (HOR) takes place at the anode, while the oxygen reduction reaction (ORR) occurs at the cathode. These electrodes are separated by an electrolyte, a material that conducts ions but not electrons. For the transport of reactants in ionic form through an aqueous electrolyte from the one electrode to the other, where then water molecules are formed, two types of ions are possible: positively charged protons (H^+) or negatively charged hydroxide ions (OH^-). The type of ion depends on the operating conditions and the medium, specifically whether the reactions occur under acidic or alkaline conditions [30]. Consequently, the half-reactions at the electrodes vary with the pH of the environment.

Under acidic conditions, the half-reactions are:

$$2\,H_2 \longrightarrow 4\,H^+ + 4\,e^- \qquad \text{HOR} \tag{3.2}$$

$$O_2 + 4\,H^+ + 4\,e^- \longrightarrow 2\,H_2O \qquad \text{ORR} \tag{3.3}$$

In an alkaline environment, they are described as:

$$2\,H_2 + 4\,OH^- \longrightarrow 4\,H_2O + 4\,e^- \qquad \text{HOR} \tag{3.4}$$

$$O_2 + 2\,H_2O + 4\,e^- \longrightarrow 4\,OH^- \qquad \text{ORR} \tag{3.5}$$

The dependence of the half-reactions on pH clearly illustrates that different approaches exist for FC design. This observation forms the basis for the following chapter. However, the energy released by the overall reaction does not change with the choice of half-reactions, and therefore, all designs operate

under the same fundamental thermodynamic constraints. From equation 2.6, it follows that the theoretical cell voltage of a hydrogen FC is determined by the Gibbs free energy for the formation of water according to equation 3.1. Under standard conditions, this corresponds to a value of 1.23 V, independent of pH. This represents the theoretical maximum voltage that can occur in hydrogen-based FCs. The theoretical maximum efficiency η_{max} of a FC is defined as the ratio of the Gibbs free energy of formation ΔG_f to the standard enthalpy of formation of the reactants ΔH_f, expressed as:

$$\eta_{max} = \frac{\Delta G_f}{\Delta H_f} \tag{3.6}$$

Assuming that the water produced in equation 3.1 is obtained in liquid form under standard conditions, the maximum efficiency of a hydrogen FC is $\eta_{max} = 83\%$ [30]. This theoretical efficiency is significantly higher than that of a conventional heat engine, providing a strong motivation for the use of FCs in electrical energy generation [31]. Nevertheless, practical implementations of FCs experience efficiency losses, as the maximum cell voltage of 1.23 V cannot be achieved in real systems. As discussed in section 2.1, this reduction in cell voltage is primarily attributed to so-called overpotentials. Consequently, the cell voltage serves as a reliable indicator of FC efficiency. The four main factors contributing to overpotentials in FCs can be described as follows [30]:

- **Activation losses**: These losses arise because for the half-reactions at the electrodes to occur, they must overcome energy barriers, the activation energy. Although this barrier can be reduced by selecting an appropriate catalyst, as discussed in section 2.2, it is very difficult to be completely eliminated. Furthermore, according to the Butler–Volmer equation (equation 2.11), activation losses strongly depend on the material-specific exchange current density. Due to the non-linear relationship, they have a particularly significant impact on the overpotential at low current densities.

- **Internal currents and fuel crossover**: These losses typically occur in practical systems and result from the fact that, although the electrolyte is designed to conduct only ions, its insulating properties are rarely perfect. Consequently, a small fraction of electrons may pass through the electrolyte instead of the external circuit, or reactants may cross over to the opposite electrode. The latter is further facilitated by the high volatility of hydrogen. In both cases, electrons transferred during the reaction are no longer available for useful work.

- **Ohmic losses**: These losses are associated with a linear drop in potential as current density increases and originate from resistances within the FC. Both electric resistance between electrode components and ionic resistance within the electrolyte contribute to this effect, although the latter one typically dominates these kinds of losses.

- **Mass-transport losses**: These losses occur at very high current densities when reactants can no longer be supplied to the electrodes or products

removed from the electrode at a sufficient rate. The resulting change in reactant concentration leads, according to the Nernst equation (equation 2.8), to a deviation of the cell voltage and thus an additional overpotential.

Each of the loss mechanisms affects cell voltage in different current density ranges. These effects can be visualized using a polarization curve, which plots cell voltage against current density. Such a representation allows the distinct regions dominated by the respective losses to be easily identified. Therefore, polarization curves provide a practical tool for quickly diagnosing the causes of efficiency losses. A typical polarization curve for a hydrogen FC, including the regions corresponding to the different sources for the overpotential, is shown in Figure 3.2. The relative magnitude of the various sources of overpotential is highly dependent on the type of fuel cell and, above all, the resulting operating conditions.

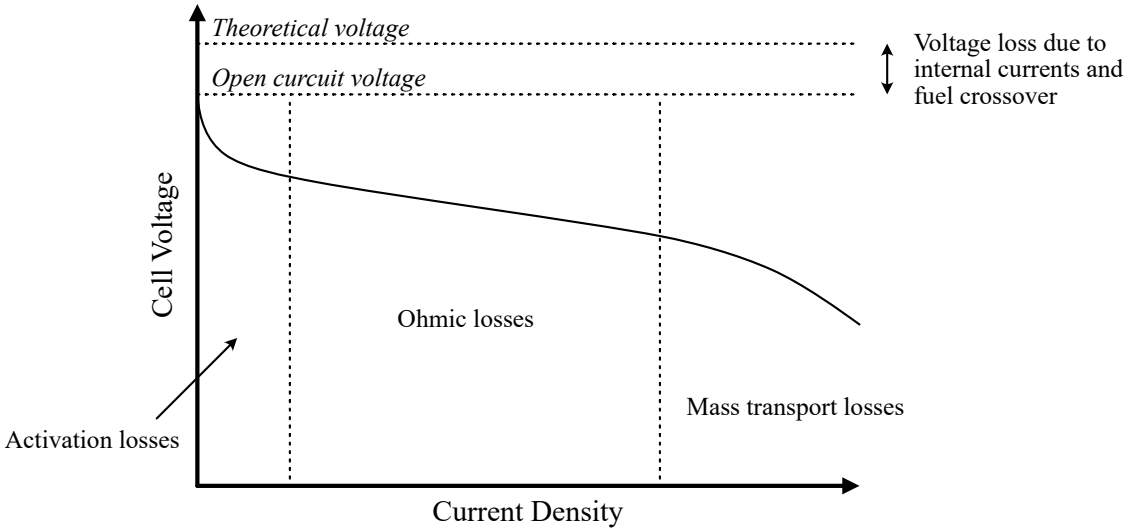

Figure 3.2: Generic polarization curve for a typical hydrogen FC operating at low temperatures and air pressure.

3.3 Types of Fuel Cells

The choice of design of the FC can, as previously discussed, allow for a wide range of different FC types, even though the fundamental operating principle remains the same. Among all design parameters, the selection of the electrolyte material exerts the greatest influence. Its selection dictates the operating conditions of the FC, which in turn determine the suitable materials for the other FC components. Moreover, as outlined in Section 3.2, the electrolyte strongly affects the reaction environment, such as for example acidic or alkaline conditions, which ultimately determines the type of charge carriers and, consequently, the associated half-reactions [30]. For this reason, many FC types are primarily classified according to the nature of their electrolyte. The most common fuel cell types include polymer membrane-based systems such as

proton exchange membrane fuel cell (PEMFC) and anion exchange membrane fuel cell (AEMFC). Other variants, such as phosphoric acid fuel cell (PAFC) and alkaline fuel cell (AFC), employ aqueous acidic or alkaline electrolytes. In addition, high-temperature systems like molten carbonate fuel cell (MCFC) and solid oxide fuel cell (SOFC) operate under entirely different conditions [32]. Unlike the previously mentioned types, these high-temperature fuel cells use charge carriers that do not rely on the ionic conduction of water-based species. Instead, they employ alternative ionic conduction mechanisms such as carbonate or oxide ion transport, which require elevated temperatures for effective operation [30, 33]. An overview of the differences between these FC types is provided in Table 3.1.

FC type	PEMFC	AEMFC	PAFC	AFC	MCFC	SOFC
Electrolyte	Polymer	Polymer	Phosphoric Acid	Potassium hydroxide	Molten carbonate	Ceramic
Charge carrier	H^+	OH^-	H^+	OH^-	${CO_3}^{2-}$	O^{2-}
Operating temperature	20–100 °C	60–100 °C	150–200 °C	50–200 °C	650 °C	500–1000 °C
Application	Transport, backup power	Transport, backup power	Integrated heat and power systems	Space vehicles	Integrated heat and power systems	Integrated heat and power systems

Table 3.1: List of the key parameters of the most common hydrogen FC types. Data from [30, 33–35].

Differences in the design of various FC types naturally lead to different application areas. Two of the key factors are the physical state of the electrolyte and the operating temperature of the FC. For example, systems that employ liquid electrolytes, such as PAFC and AFC, are generally less suitable for mobile applications, as electrolyte management and the associated balance-of-plant requirements increase system complexity. Similarly, FCs that operate at high temperatures, such as MCFC and SOFC, are less practical for transportation as they require extended start-up and shut-down times [34, 36]. However, in stationary applications, these high temperature systems enable efficient combined heat and power operation, allowing the generated waste heat to be utilized for space heating and hot water production.

In contrast, membrane-based FCs are particularly well suited for use in the transportation sector, i.e. mobile applications [30, 32]. Their solid electrolyte membranes make them easier to handle and allow for flexible operation at relatively low temperatures. In addition, their compact design and associated high energy density make them strong candidates for mobile applications,

especially for heavy-duty transport powered by FCs. As a result, polymer electrolyte-based FCs are of particular relevance to this work and will therefore be the primary focus in the following sections. Nevertheless, all FC types share a fundamentally similar architecture with the same basic components. These components will be discussed below using PEMFC and AEMFC as examples, but with appropriate adjustments to operating conditions, the concepts can be transferred to other systems.

3.3.1 Fuel Cell Components

In its simplest form, a polymer electrolyte based FC consists of only four main components [30]. At its core lies the polymer electrolyte, which enables the separation of the half-reactions and facilitates ion transport. On both sides of the polymer membrane are the electrodes (anode and cathode), where the electrochemical reactions take place. To ensure these reactions proceed efficiently, each electrode incorporates a catalyst, which is why they are commonly referred to as catalyst layers (CLs). Together, the two CLs and the polymer membrane form the so-called catalyst coated membrane (CCM).

The CCM is bordered on both sides by so-called gas diffusion layers (GDLs), which regulate the transport of reactants and products to and from the electrodes. Finally, each GDL is adjacent to a bipolar plate (BP). These plates serve multiple functions: they distribute fuel, oxidant, and products, act as current collectors, and provide mechanical stability to the fuel cell. The individual components and their arrangement within a FC can be seen in Figure 3.3.

Polymer Electrolyte

The polymer electrolyte membrane is the component of a FC that has the greatest impact on its functionality, and the cell is therefore typically designed around this key element. Positioned at the center of the FC, the membrane acts as a physical barrier between the two electrode compartments. To enable this separation, the membrane must be made of a semipermeable polymer material with a very high intrinsic electrical resistance, ensuring that electrons released during the half-reactions cannot take a direct path to the opposite electrode [37]. Semipermeability of the membrane is also essential to minimize direct crossover of reactants, allowing them to pass through the polymer only in ionic form. At the same time, the polymer must exhibit excellent chemical, mechanical, and thermal stability to prevent material failure under the harsh operating conditions inside the FC [30, 37, 38].

Such an ion-conducting polymer is referred to as an ionomer and typically consists of a chemically resistant polymer backbone with functional side chains attached [30, 37]. Depending on the type of polymer electrolyte, these functional groups terminate in either acidic or basic moieties. Since the functional groups are generally hydrophilic, while the backbone is largely hydrophobic, ionomers form a characteristic phase-segregated macrostructure in which these regions organize relative to each other. As a result, hydrophilic and hydrophobic domains develop within the polymer. The hydrophilic regions can absorb

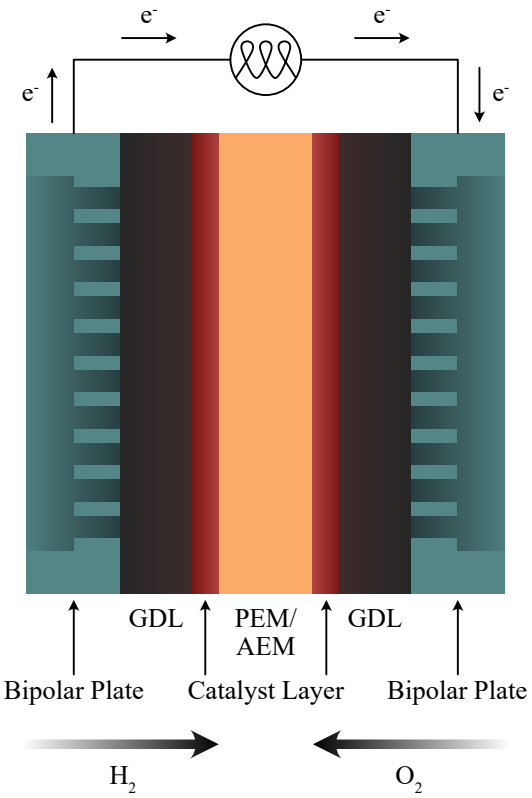

Figure 3.3: Schematic illustration of a polymer electrolyte FC with labels for the main components.

water, creating water-filled domains that, if sufficiently interconnected, form channels [30, 37]. A schematic drawing of the channel structure can be seen in Figure 3.4a. Within these channels, the environment is strongly acidic or strongly basic, depending on the functional groups, meaning that either positively charged protons (H^+) or negatively charged hydroxide ions (OH^-) are present in solution. If the membrane is adequately hydrated, these ions can migrate through the channels in the polymer membrane, while the material remains largely impermeable to other molecular species. Ion transport within these channels occurs via several mechanisms. The most significant mechanisms are vehicular diffusion and the much faster and therefore dominant Grotthuss mechanism. While vehicular diffusion involves the physical movement of H_3O^+ or OH^- ions along the concentration gradient between the electrodes, the Grotthuss mechanism describes the transfer of protons through successive hydrogen-bond rearrangements, effectively enabling charge migration via proton "hopping" along a hydrogen-bonded water network. Under typical operating conditions, this combination of mechanisms ensures sufficient ionic conductivity in this type of ionomer [30, 37, 39].

As previously mentioned, the nature of the functional groups determines whether the ionomer can conduct H^+ or OH^-. Consequently, the chemical structure of the ionomer also dictates the type of polymer electrolyte membrane FC in which it can be used. This material class was first synthesized by Donald J. Connolly and Walther Grot in the 1960s when they developed Nafion [40]. Nafion serves as a proton exchange membrane (PEM) and has since then been

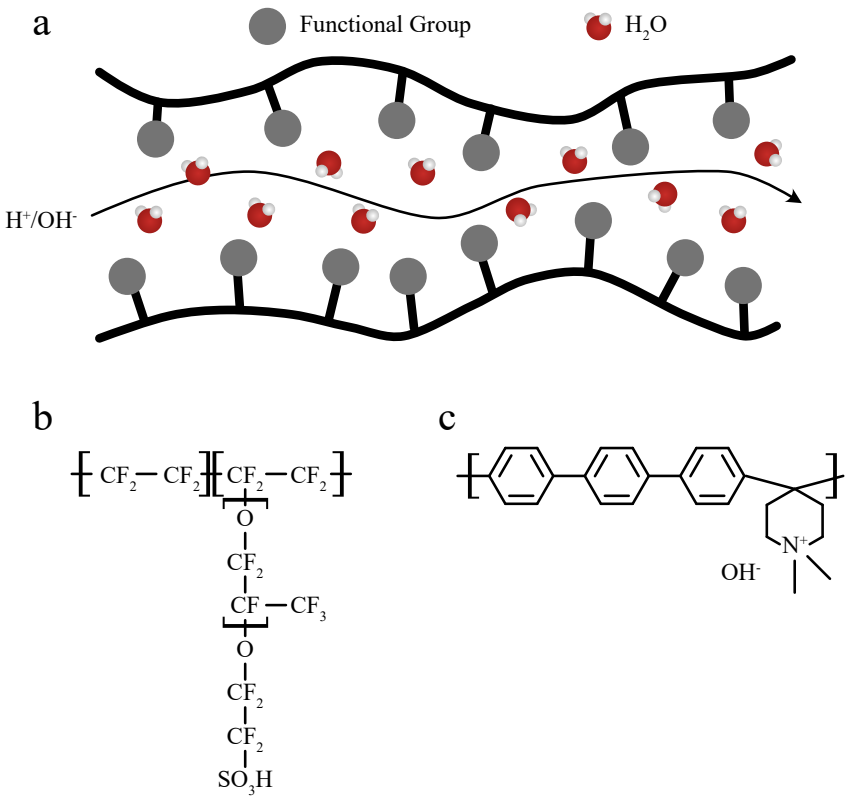

Figure 3.4: a) Schematic illustration of the water channel structure in a polymer electrolyte membrane. b) Chemical structure of Nafion, a proton exchange membrane material. c) Chemical structure of QAPPT, an anion exchange membrane material.

widely employed in the development of PEMFC systems. It belongs to the class of perfluorosulfonic acid (PFSA) polymers, meaning its backbone consists of polyfluorinated alkyl chains from which side chains with sulfonic acid end groups branch off as hydrophilic centers [37, 41]. The length of the backbone and the side chains can be varied, which in turn influences the macrostructure and the channels responsible for H^+ transport. The chemical structure of Nafion is shown in Figure 3.4b. Ionomers from the PFSA class can generally be used very reliably in PEMFC systems due to their outstanding stability and ionic conductivity. However, the toxicity associated with perfluorinated substances [42, 43] has led to increasing efforts to replace these polymers with alternatives based on chemically resistant hydrocarbon backbones, such as aromatic ethers or ketones, although FCs employing these alternatives often fail to achieve a similar performance as those using PFSA-based materials [37, 44].

While Nafion and Nafion-like polymers are already widely used as a standard in PEMFCs, the situation for AEMFCs is less clear. For the class of anion exchange membranes (AEMs), several chemical strategies currently exist to enable OH^- conduction. Although the backbone in AEMs can also be formed from polyfluorinated alkyl chains, many other structures are under discussion, including polyetherketones, polyphenylenes, and polybenzimidazoles [44, 45]. In

the latter case, the cationic groups are an integral part of the polymer backbone, whereas most other frameworks employ side chains that carry the functional groups. For AEMs, these functional groups must exhibit basic character, which is why nitrogen-based groups are commonly used. Examples include quaternary ammonium groups such as benzyltrialkylammonium, as well as heterocyclic groups like benzimidazolium or polybenzimidazolium [45]. Phosphorus-based systems are also being considered, although being less prevalent. Due to the numerous possible combinations, there are many different candidates for AEMs, and an exemplary structure is shown in Figure 3.4c. The limited adoption of AEMs, and thus AEMFCs, compared to PEMFCs is primarily connected to the chemical instability of the polymer backbone under highly alkaline conditions on the one hand and the lower mobility of OH^- compared to H^+ on the other hand [45, 46]. The latter in particular poses a major challenge since, although fully hydrated AEMs can sometimes achieve ionic mobilities comparable to Nafion, this performance strongly depends on the degree of hydration, which complicates practical implementation in FCs. Furthermore, it is important to note that AEMs are highly sensitive to even small amounts of CO_2 in the reactant gases [47].

Catalyst Layer

CLs form the electrodes of a fuel cell, where the electrochemical reactions take place: the HOR at the anode and the ORR at the cathode. These electrodes must be designed to enable efficient electron transfer, which requires a large number of active sites where reactants can adsorb and react. A porous structure is particularly advantageous, as it provides good accessibility for gaseous reactants while offering a very high surface area. The electrode material must also exhibit excellent electrical conductivity and chemical stability under harsh reaction conditions, while, ideally, being abundant and cost-effective. In polymer-membrane-based fuel cells, carbon is commonly used as the support material. Highly porous carbon structures are employed, typically consisting of interconnected agglomerates of primary carbon particles with sizes in the range of 30 nm to 50 nm, which ensures good gas accessibility. Common examples include Vulcan or Ketjenblack, with the latter one offering a high surface-to-volume ratio of approximately $1200\,m^2\,g^{-1}$ [30, 46, 48]. However, the carbon support itself does not provide an intrinsically active surface for HOR and ORR.

As outlined before, an efficient reaction requires the presence of a catalytic surface. For this reason, the carbon support is typically decorated with catalyst material. To maximize the available active surface area, the catalyst is usually applied in the form of nanoparticles (NPs). The particle size depends on the catalyst material, with platinum commonly being used in PEMFCs and AEMFCs. Here, the platinum NPs typically have a diameter of only around 3 nm, which helps to maximize the surface-to-volume ratio [30, 46, 48]. This is important as bulk sites cannot act as an active site for the reaction. This consideration is particularly critical for platinum, given its high cost and scarcity. For the same reason, achieving a uniform distribution and good dispersion

of catalyst particles on the carbon support is essential. Therefore, significant research efforts focus on optimizing catalyst utilization and minimizing the amount required, especially for expensive materials, providing strong motivation for innovation. Various strategies have been explored, such as alloying, although the specific possible catalysts in PEMFCs and AEMFCs will be discussed in detail in the corresponding sections.

To complete the structure of the CL, one final component is required, since the protons (or hydroxide ions) generated during the reaction must be transported between the catalyst and the membrane. To enable efficient ionic conduction, an ionomer is typically incorporated into the CL. The ionomer serves both as a binder and as an interface to the membrane, and, in practice, this means that the catalyst surface is usually coated with a thin ionomer film [30]. However, this coating competes with gas accessibility, as ionomers are inherently poorly permeable to gases. Therefore, achieving an optimal ratio between ionomer and carbon is a critical aspect of CL fabrication. A schematic representation of the structure of a typical CL is shown in Figure 3.5.

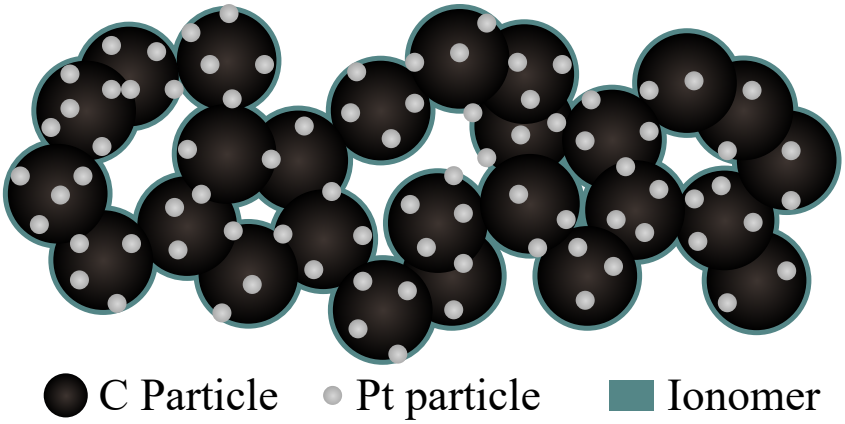

Figure 3.5: Schematic drawing of an idealized structure of a polymer electrolyte FC.

A reaction within the CL can only occur when the catalyst surface, reactant gases, and either H^+ or OH^- ions are simultaneously available. These points, where these three distinct phases meet, are commonly referred to as the triple-phase boundary (TPB) [49]. Maximizing the TPB density is essential, but the interactions between the different components must also not be underestimated. During operation, strong adhesion of catalyst particles to the support and good electronic contact are crucial, while other interactions can be detrimental. For example, under unfavorable conditions, the catalyst may induce corrosion of the carbon support, reducing surface area and causing catalyst particle agglomeration [50]. The catalyst itself must also resist corrosion, as it is exposed to the harshest conditions. Interactions between the support and ionomer must also be considered, as they can affect the uniformity of the ionomer film. Ideally, the film should be thin, homogeneous, and well-connected [51]. Furthermore, the interaction between ionomer and catalyst is particularly critical, as this interface governs ion transport while potentially inhibiting reaction sites by blocking the surface. Additionally, the ionomer can influence the catalyst

surface through poisoning effects, while the catalyst surface in turn can also alter the ionomer's structure [52]. Because the structure of the ionomer directly impacts ionic conductivity, such changes can have far-reaching consequences.

Finally, water management within the CL is another decisive factor influencing the design choices. Adequate hydration of both the ionomer and the membrane must be maintained, while excess water produced during operation must be efficiently removed to prevent electrode flooding, as flooding reduces gas accessibility and impairs performance. Consequently, the CL design must strike a careful balance between hydration and water removal.

Gas Diffusion Layer

Since the focus of this thesis lies on the mechanisms within the electrodes and the ionomer, the components named gas diffusion layer (GDL) and bipolar plate (BP) will only be briefly discussed for completeness. The GDL is usually positioned directly on top of the CL and serves two primary functions: the GDL has to ensure uniform distribution of reactant gases across the entire CL surface while simultaneously enabling efficient removal of the produced water, and providing optimal electrical contact between the CL and the current collector. To fulfil these roles, GDLs are typically made from carbon-based materials such as carbon paper. Their high porosity guarantees effective gas distribution, while carbon itself provides excellent electrical conductivity. To facilitate water removal and enhance chemical stability, GDLs are commonly treated with polytetrafluoroethylenes (PTFEs). On the side of the GDLs facing the CLs, it is standard practice to apply a microporous layer (MPL), which further improves electrical contact and reactant distribution. The MPL usually consists of high-surface-area carbon, similar to that used in the CLs, and is also often treated with PTFEs [30].

Bipolar Plates

BPs are typically made from graphite or stainless steel and serve as both current collectors and mechanical stabilizers. In addition, they are designed to create flow fields for the reactant gases. The exact geometry of these flow fields depends on various parameters and can differ between the anode and cathode sides. Another key requirement for BP materials is high thermal conductivity, as the waste heat generated by the fuel cell is primarily dissipated through the BPs. Since a single fuel cell can only deliver a limited amount of power, FC systems generally consist of multiple cells stacked together and electrically connected in series. This configuration, known as a fuel cell stack, enables significantly higher power output. The BPs then separate the individual cells within the stack while maintaining electrical and mechanical integrity. However, the focus of this thesis will be restricted to the mechanisms within a single FC [30].

3.3.2 Proton-Exchange Membrane Fuel Cell (PEMFC)

PEMFCs represent the most widely used and thoroughly researched type among the two polymer membrane fuel cell technologies introduced previously. This is primarily due to the advanced development and high efficiency of PEMs. As a result, PEMFCs have already found commercial applications in mobile systems within the transportation sector, for example in vehicles produced by manufacturers such as Toyota, Hyundai, Honda, Mercedes-Benz, and General Motors.

Since the operation of a PEMFC relies on proton conduction within the PEM, the electrochemical reactions occur in a strongly acidic environment. At the anode, the HOR takes place on the catalyst surface according to equation 3.2, where hydrogen molecules are split into protons and electrons. The electrons are conducted through the external circuit, while the protons are transported across the PEM. In general, three elementary steps are considered for this reaction [53]:

$$\text{Tafel} \qquad \mathrm{H_2} + 2\,{}^{*} \longrightarrow 2\,\mathrm{H^{*}} \tag{3.7}$$

$$\text{Heyrovsky} \qquad \mathrm{H_2} + {}^{*} \longrightarrow \mathrm{H^{*}} + \mathrm{H^{+}} + \mathrm{e^{-}} \tag{3.8}$$

$$\text{Volmer} \qquad \mathrm{H^{*}} \longrightarrow \mathrm{H^{+}} + \mathrm{e^{-}} \tag{3.9}$$

Here, the symbol * denotes an active site on the catalyst surface. To obtain the overall reaction, either the Tafel or Heyrovsky step can be combined with the Volmer step. Platinum is generally considered an excellent catalyst for this reaction. With highly active catalysts such as platinum, both the Tafel–Volmer and Heyrovsky–Volmer pathways exhibit very low activation energies, which means the HOR will proceed rapidly and require only small overpotentials [54]. Thus, the HOR generally accounts for comparatively small contributions to voltage losses within a PEMFC.

The situation is markedly different for the ORR at the cathode. Under acidic conditions, the ORR is significantly more complex than the HOR, and two distinct reaction pathways are possible, where one involves two electrons being transferred in two reactions, and another involving four electrons being transferred in a single reaction. The direct four-electron pathway has already been introduced in equation 3.3. However, it is also possible for oxygen and protons to react via an intermediate step involving $\mathrm{H_2O_2}$, which is subsequently reduced to water in a second step [55]:

$$\mathrm{O_2} + 2\,\mathrm{H^{+}} + 2\,\mathrm{e^{-}} \longrightarrow \mathrm{H_2O_2} \tag{3.10}$$

$$\mathrm{H_2O_2} + 2\,\mathrm{H^{+}} + 2\,\mathrm{e^{-}} \longrightarrow 2\,\mathrm{H_2O} \tag{3.11}$$

This indirect pathway is undesirable in PEMFCs, since it delivers a lower potential and current compared to the direct four-electron route. More importantly, the formation of $\mathrm{H_2O_2}$ in a PEMFC should be avoided whenever possible, as $\mathrm{H_2O_2}$ tends to generate radical species that can cause degradation of the

PEM [56]. Since the occurrence of H_2O_2 cannot be completely eliminated, modern PEMs often incorporate radical scavengers to mitigate these effects.

For the direct four-electron ORR pathway, two distinct reaction mechanisms are proposed, one dissociative mechanism and one associative mechanism [57]. In the dissociative mechanism, oxygen molecules first dissociate on the catalyst surface, as suggested by the name, and subsequently react with protons from the ionomer to form OH adsorbed on the catalyst surface, which then further reacts to H_2O in a subsequent step:

$$O_2 + 2\,{}^* \longrightarrow 2\,O^* \tag{3.12}$$

$$O^* + H^+ + e^- \longrightarrow OH^* \tag{3.13}$$

$$OH^* + H^+ + e^- \longrightarrow H_2O + {}^* \tag{3.14}$$

In the associative reaction mechanism, adsorbed oxygen molecules do not dissociate immediately on the catalyst surface. Instead, they react with protons from the ionomer to form an adsorbed OOH intermediate. This intermediate then reacts with another proton to produce water, leaving behind an adsorbed oxygen atom on the catalyst surface. This remaining oxygen atom subsequently undergoes the same sequence of steps as in the final two stages of the dissociative mechanism, in the end forming another water molecule:

$$O_2 + {}^* \longrightarrow {O_2}^* \tag{3.15}$$

$${O_2}^* + H^+ + e^- \longrightarrow OOH^* \tag{3.16}$$

$$OOH^* + H^+ + e^- \longrightarrow O^* + H_2O \tag{3.17}$$

$$O^* + H^+ + e^- \longrightarrow OH^* \tag{3.18}$$

$$OH^* + H^+ + e^- \longrightarrow H_2O + {}^* \tag{3.19}$$

Which mechanism ultimately dominates during PEMFC operation depends on the chosen catalyst and the applied potential. Similar to the HOR, the kinetics of the ORR can be significantly improved by using platinum as a catalyst, and platinum or platinum-based alloys are frequently employed [48]. This is particularly important because the ORR remains much slower than the HOR due to its more complex reaction mechanism. Therefore, the cathode exhibits substantially higher overpotentials than the anode, accounting for the majority of activation losses in a PEMFC [58]. As discussed in Chapter 2.2, the reaction kinetics on different catalyst materials can be correlated with the binding energy of a key reactant species to the catalyst using a volcano plot. For the ORR, the oxygen binding energy serves as the descriptor, and the corresponding volcano plot is shown in Figure 3.6. This plot illustrates that platinum provides the highest activity among pure metals, yet its oxygen binding energy remains slightly higher than the optimal value [57]. The PEMFC performance can be increased by loading the cathode with a larger amount of platinum NPs or, alternatively, alloying platinum with other elements can help close this gap and achieve improved activity [59]. Given the cost and scarcity

of platinum, practical applications require a compromise between performance and cost. This, in turn, creates a strong incentive to, on the one hand, enhance catalyst activity through approaches such as alloy development and, on the other hand, increase the catalyst utilization by cathode design optimization. Consequently, a significant portion of PEMFC-related research focuses on improving the kinetics of the ORR.

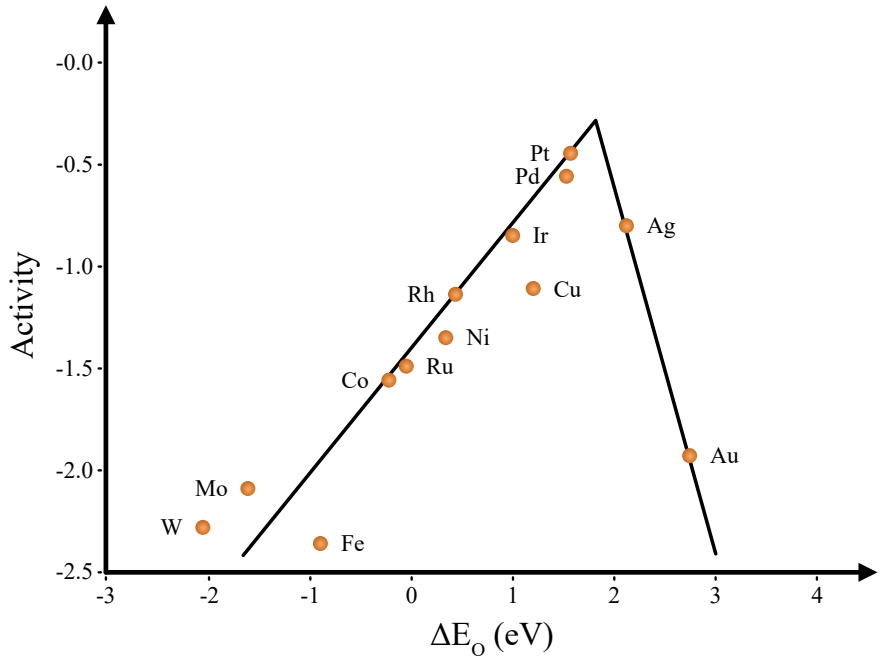

Figure 3.6: Volcano plot for the ORR reaction with the most common catalyst materials in dependence of their oxygen binding energy. The data was retrieved from [57].

Another major research area in PEMFC technology focuses on the durability of these systems. The various components of a PEMFC are exposed to harsh operating conditions, which generally leads to gradual degradation. In particular, the combination of strongly acidic conditions and high electrode potentials, especially at the cathode, places severe stress on materials, causing corrosion and deactivation. As mentioned earlier, the PEM is highly susceptible to attack by radical species. These radicals typically target functional side chains or terminal ends of the polymer backbone, significantly impairing the ionomer's functionality and, consequently, proton transport from the anode to the cathode [56]. Another source of performance loss is the reduction of the ECSA of the catalyst at the electrodes [50, 60]. Since the generated current is directly proportional to the surface available for the reaction, any decrease in the ECSA has a direct impact on the maximum power output of the PEMFC. There exist several mechanisms contributing to this phenomenon. The most common include growth of platinum NPs through Ostwald ripening or migration followed by coalescence, as well as material loss due to particle detachment from the support or gradual dissolution of particles. Particle growth leads to a reduction of the surface-to-volume ratio, limiting effective catalyst material

utilization. Processes such as Ostwald ripening and dissolution are strongly influenced by changes in cell voltage and the associated electrode potential. Depending on the applied potential, the platinum surface may be either in an oxidized or reduced state. Dynamic operating conditions cause frequent shifts in cell voltage, which in turn leads to repeated changes in the oxidation state of the catalyst surface, which has been identified as a key driver of catalyst dissolution [61]. Other mechanisms, particularly those involving loss of contact between the NPs and the support (e.g., migration or detachment), can be exacerbated by carbon support corrosion [50, 62]. Oxidation of the carbon support to carbon dioxide alters the morphology of the primary carbon particles on which the platinum NPs are anchored. Furthermore, the loss of the porous secondary structure of the support can impede gas access or disrupt electrical connectivity within the electrode [63]. Corrosion can also occur in BPs and other components, however, this thesis primarily focuses on degradation processes within the electrode structure.

3.3.3 Anion-Exchange Membrane Fuel Cell (AEMFC)

AEMFCs are currently less developed and therefore less widespread compared to PEMFCs. This is noteworthy given that alkaline fuel cells were considered state-of-the-art in the mid-20th century and were even used in space applications [64]. However, they were eventually replaced with membrane-electrolyte systems, which offer significant structural advantages. The first ion-conducting polymers developed were all proton-conducting (PEMs), as proton transport through an ionomer is generally easier to achieve. Moreover, the mobility of H^+ in PEM materials such as Nafion is substantially higher than that of OH^- in AEM materials [44]. Consequently, research interest in AEM technology remained relatively low for a long time. Nevertheless, operating a fuel cell under alkaline conditions offers the decisive advantage that the less corrosive environment and lower electrode potentials allow for the use of alternative catalyst materials. More importantly, these milder conditions enable the use of catalysts that do not belong to the platinum group or other noble metals, potentially reducing costs dramatically compared to the expensive platinum NPs required in PEMFC CLs.

Due to the different conditions at the electrodes, the elementary reactions also differ, as shown in equations 3.4 and 3.5. Under alkaline conditions, water is formed at the anode during the HOR, which complicates the reaction mechanism. Similar to the acidic case, two combinations of three elementary steps are generally considered here [65]:

$$\text{Tafel} \qquad H_2 + 2\,{}^* \longrightarrow 2\,H^* \tag{3.20}$$

$$\text{Heyrovsky} \qquad H_2 + OH^- + {}^* \longrightarrow H^* + H_2O + e^- \tag{3.21}$$

$$\text{Volmer} \qquad H^* + OH^- \longrightarrow H_2O + e^- + {}^* \tag{3.22}$$

As under acidic conditions, the HOR under alkaline conditions can proceed via either the Tafel–Volmer or Heyrovsky–Volmer combination. However,

in both the Heyrovsky and Volmer step, the formation of water molecules involves an additional species, OH^-. Whether this hydroxide ion is adsorbed on the catalyst surface during the reaction or remains in solution is not always conclusively determined and largely depends on the nature of the catalyst surface. For platinum-based catalysts, it is generally assumed that only solvated OH^- participates in the reaction [66]. This implies that hydrogen desorption from the catalyst surface is the rate-limiting step. Therefore, the catalytic activity is strongly influenced by the binding energy of hydrogen to the surface, also called the hydrogen binding energy (HBE). Since the HBE of hydrogen increases with rising pH, the HOR kinetics on platinum under alkaline conditions are several orders of magnitude slower than under acidic conditions [67]. As a result, the HOR contributes significantly to overpotentials and activation losses in AEMFCs. This has led to increased research efforts focused on developing and tailoring catalysts for HOR in alkaline environments. Similar to PEMFCs, strategies include replacing platinum with other metals exhibiting comparable electrocatalytic properties. Palladium is one such candidate, although its HOR mechanism is not fully understood due to palladium's ability to absorb hydrogen into its crystal lattice. However, combining palladium with transition metal oxides can enable OH^- adsorption on the oxide surface, which, if followed by spillover to the palladium surface, can enable HOR activities comparable to those of platinum-based systems [68].

While the HOR is generally slower in AEMFCs than in PEMFCs, the opposite is true for the ORR under alkaline conditions. Here, again two pathways are possible, the direct four-electron route described in equation 3.5, and a two-electron route involving two steps, with HOO^- as an intermediate [69]:

$$O_2 + H_2O + 2\,e^- \longrightarrow HOO^- + OH^- \tag{3.23}$$

$$HOO^- + H_2O + 2\,e^- \longrightarrow 3\,OH^- \tag{3.24}$$

The exact reaction mechanism under these conditions is far less understood than in acidic environments. However, it is generally assumed that the first electron transfer from the catalyst surface to adsorbed O_2, forming $O_2{}^-$, represents the rate-limiting step for the ORR [70]. More importantly, the kinetics of the ORR strongly depend on the pH of the environment, with overpotentials decreasing as pH increases [71]. Consequently, the ORR proceeds much more facile in AEMFCs and contributes less to overall activation losses compared to PEMFCs. This opens up the realistic possibility of using alternative catalyst materials for the ORR instead of platinum. In fact, more abundant materials such as palladium and silver, or even transition-metal-based catalysts containing iron, cobalt, or manganese, can be used [72].

Since AEMFCs are still in an earlier stage of development compared to PEMFCs, research on their durability is far less extensive. Moreover, most degradation studies focus primarily on the AEM, as its failure typically causes greater performance loss than CL degradation or corrosion. As previously mentioned, the limited lifetime of AEMs can be attributed to several factors,

including high sensitivity to hydration fluctuations and increased ionic resistance due to carbonation from CO_2 contamination [45]. This contamination can originate from ambient air used as the oxidant or from internal oxidation of carbon components within the cell. Chemical degradation of the polymer also plays a critical role, as AEMs are generally less resistant than the fluoropolymers used in PEMFCs. As a result, AEMs or ionomers within the CL typically fail before significant electrode or catalyst degradation occurs, especially when platinum or palladium-based catalysts are used. Nevertheless, the few available studies indicate that CL degradation mechanisms in AEMFCs are broadly similar to those in PEMFCs, including ECSA loss due to Ostwald ripening, migration followed by coalescence, or simple detachment and dissolution of NPs [47]. Coalescence and detachment appear particularly relevant in AEMFCs, as platinum and platinum-like catalysts tend to enhance carbon support corrosion under alkaline conditions. Interestingly, protective coatings of transition metal oxides have been shown to significantly slow ECSA loss, as demonstrated for palladium supported on CeO_2 over carbon [73].

Chapter 4

Applied Methods

This chapter discusses all methods employed in this thesis. The focus is on providing a general introduction to these methods, while detailed information about experimental procedures can be found in the appended papers.

4.1 Electrochemical Measurements

Since fuel cells can generally be described as electrochemical systems, the first part of this chapter addresses possibilities for characterizing electrochemical processes. To this end, the studies on which this thesis is based involve electrochemical measurements that were combined with complementary analytical methods.

4.1.1 Electrochemical Characterization

The simplest approach to electrochemical characterization of a redox reaction is often direct measurement in an electrochemical setup. In its most basic form, as described in Chapter 2.1, this setup consists of two electrodes immersed in an electrolyte solution, with one serving as the anode and the other as the cathode hosting the two half-reactions. When a potential is applied, a resulting current can be measured. Conversely, applying a current allows the measurement of the corresponding potential. In this configuration, one electrode acts as the working electrode (WE), where the half-reaction of interest occurs, while the other serves as the counter electrode (CE). However, reliably determining the electrode potential of the WE in a two-electrode system is not always possible. Therefore, electrochemical measurements typically employ a reference electrode (RE) with a well-defined potential. Introducing this third electrode creates the so-called three-electrode setup, in which the potential of the WE is measured relative to the RE, while the current flows between the WE and the CE. Control and measurement of potential and current in such setups are usually performed using an instrument called a potentiostat. A schematic representation of this configuration is shown in Figure 4.1.

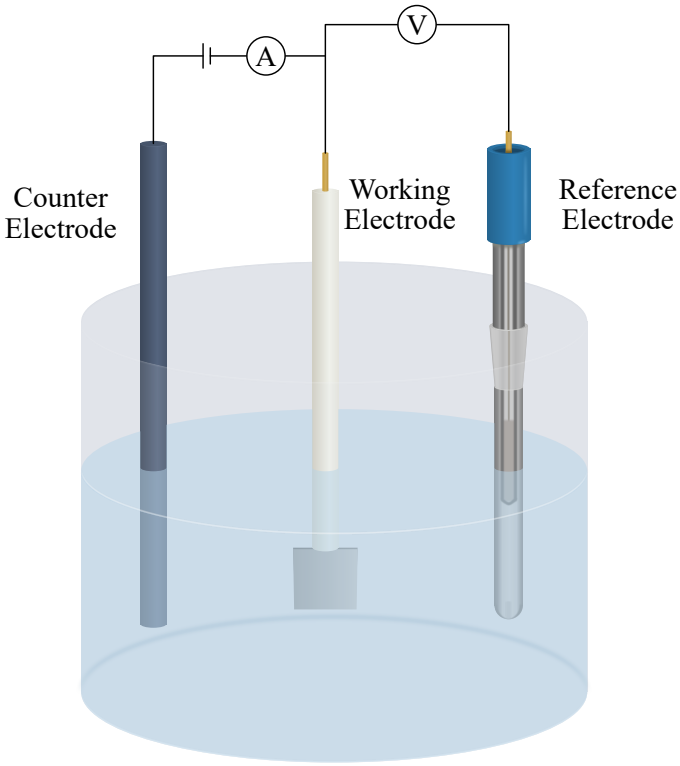

Figure 4.1: Drawing of a three-electrode setup. A platinum plate is often used as WE and a graphite rod as the CE.

In such a setup, a wide range of electrochemical techniques can be employed for characterization, as both current and potential can be controlled in various ways. Among all these, voltammetry is particularly well-suited for identifying electrochemical processes occurring at the electrode surface. In this technique, the system's response is measured in the form of current generated by the potential applied to the WE. Typically, the potential between the WE and the RE is swept cyclically between two predefined limits while the resulting current is recorded. Due to these cyclic potential sweeps, the method is referred to as cyclic voltammetry (CV). The measured current can then be plotted against the applied potential to produce a voltammogram. When an electrochemical reaction occurs at a specific potential during the sweep, charge transfer takes place, which is reflected in the recorded current. If the applied potential drives oxidation of a species at the WE, electrons are transferred to the WE, resulting in a positive current known as anodic current, since the WE acts as the anode in this case. Conversely, during reduction, electrons are transferred from the WE to the species, producing a negative current, referred to as cathodic current, with the WE functioning as the cathode. Because the potentials at which these reactions occur and their characteristics depend strongly on the material of the WE and the analytes present in solution, voltammograms are highly specific to the material–analyte combination. This makes CV a widely used and powerful tool for identifying material properties and electrochemical behavior.

Platinum is the most extensively studied electrode material in the FC context. Polycrystalline platinum exhibits a distinct cyclic voltammogram

due to characteristic surface processes, as shown in Figure 4.2 [74]. This particular voltammogram was recorded in 0.5 M H_2SO_4. It can be divided into three distinct regions, each corresponding to different processes at the electrode that contribute to the measured current density. Region I spans the potential range from near 0 V vs. RHE up to approximately 0.4 V vs. RHE and primarily involves hydrogen adsorption and desorption on the platinum surface. This process is often referred to as under-potential deposition (UPD) of hydrogen. The group of peaks observed in this region reflects the electron transfer associated with hydrogen UPD on the various facets of a polycrystalline platinum surface. When following the anodic sweep, i.e. the part of the curve with positive current density, toward higher potentials, Region II appears as a relatively flat section without significant peaks. This is known as the double-layer region, where the measured currents originate solely from the response of the interfacial double layer to changes in electrode charging. These currents are capacitive and do not involve charge transfer between the electrode and the electrolyte, so therefore, they are classified as non-faradaic. A similar flat region is observed also during the cathodic sweep. At potentials above approximately 0.6 V vs. RHE, peaks corresponding to the formation of an oxide layer on the platinum electrode are observed in the anodic scan, followed by a peak in the cathodic sweep resulting from the reduction of this oxide layer. These oxygen-related interactions define Region III of the voltammogram. Extending the upper potential limit beyond 1.23 V vs. RHE would result in a pronounced increase in current density due to the onset of the oxygen evolution reaction (OER). Similarly, lowering the lower potential limit below 0.0 V would enable observation of the hydrogen evolution reaction (HER).

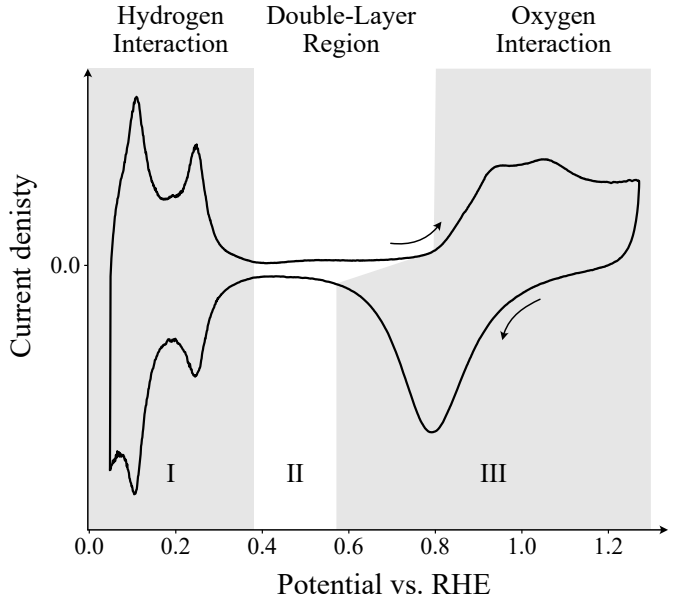

Figure 4.2: Typical cyclic voltammogram of a platinum WE in oxygen-free 0.5 M H_2SO_4. The scan directions for the anodic and cathodic sweep are indicated with arrows.

The intensity of the peaks in a voltammogram, when considered together

with the scan rate ν, provides information about the charge transferred during a scan. This relationship between current I and charge Q can be expressed as:

$$Q = \frac{1}{\nu} \int I \, dE \tag{4.1}$$

where E denotes the electrode potential. Integrating the charge associated with specific faradaic processes reveals a strong dependence on the available ECSA of the electrode. Particularly for adsorption and desorption processes, such as hydrogen UPD, the charge can be readily associated with the surface, since typically only a monolayer is adsorbed/desorbed. Consequently, the ECSA of an electrode is commonly determined from these peaks. For this calculation, it is assumed that the hydrogen coverage is 77% and that the theoretical charge required to adsorb a monolayer of hydrogen on platinum is $\theta_{\mathrm{H-Pt}} = 210\,\mu\mathrm{C\,cm^{-2}}$ [75]. Based on these assumptions, the estimated ECSA from hydrogen UPD can be calculated as:

$$A_{\mathrm{ECSA}} = \frac{Q_{\mathrm{H}}}{0.77\theta_{\mathrm{H-Pt}}} \tag{4.2}$$

In principle, the determination of ECSA is not limited to hydrogen adsorption or desorption peaks. A similar approach can be applied using CO-monolayer oxidation, although this requires a modified experimental setup and slightly different assumptions [76].

4.1.1.1 Electrochemical Quartz-Crystal Microbalance with Dissipation Monitoring (EQCM-D)

To further expand the possibilities for analyzing electrochemical systems, electrochemical characterization methods can be combined with additional, complementary techniques. One such technique is the quartz crystal microbalance (QCM). The QCM is widely used for detecting minute variations in mass and relies solely on the piezoelectric properties of quartz crystals. These properties cause the crystal lattice of a quartz crystal to deform under an applied electric field. When two electrodes are positioned on opposite sides of an AT-cut quartz crystal as illustrated in Figure 4.3, applying a voltage across the electrodes induces a shear deformation of the crystal. Consequently, applying an alternating voltage at the electrodes causes the quartz crystal to oscillate mechanically, generating a shear wave whose frequency depends on the applied alternating voltage. At a specific frequency, i.e. when half the acoustic wavelength of the shear wave equals the thickness of the quartz disk, a standing wave forms within the crystal, and the system resonates, which is evident from a significantly increased oscillation amplitude [77]. In addition to the fundamental resonance frequency, standing waves also occur at odd multiples of this frequency, referred to as overtones.

The dependence of the resonance frequency on the crystal thickness ultimately enables gravimetric measurements using this technique. When an additional layer of material is deposited on the quartz crystal, the overall thickness changes, altering the resonance conditions and thus causing a shift in

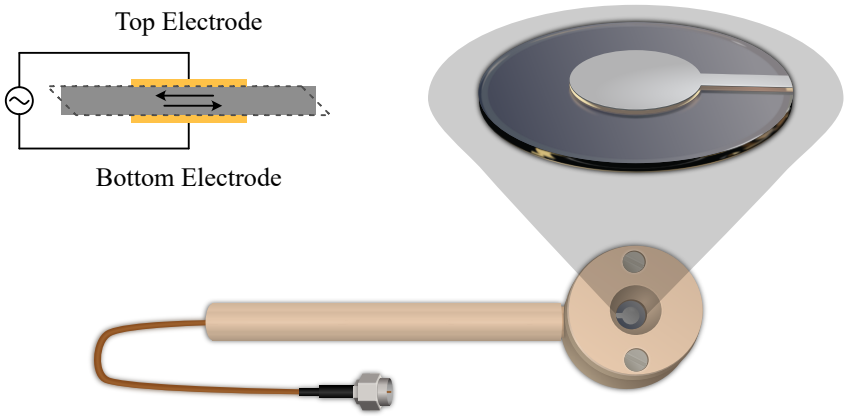

Figure 4.3: Schematic illustration of an electrochemical quartz crystal microbalance with dissipation monitoring device. In the top right corner, the working principle of the quartz-sensor is illustrated with the arrows indicating the shearing motion of the oscillation. In the bottom of this illustration the dip-holder is shown that was used to install the quartz crystals so that only the top electrode is exposed.

the resonance frequency. This added layer can be considered an extension of the quartz crystal if three fundamental conditions are met [78]: the layer must be rigidly attached to the crystal surface, and the additional mass must be uniformly distributed and negligible compared to the mass of the quartz crystal ($< 2\%$). If these conditions are satisfied, a change in resonance frequency Δf_n can be directly related to a mass change Δm using the density of quartz ρ_q. This relationship was first established by Günter Sauerbrey and is expressed in the equation named after him [78, 79]:

$$\Delta f_n = -n \frac{2 f_{0,n}^2}{A \sqrt{\rho_q \mu_q}} \Delta m \tag{4.3}$$

with the resonance frequency $f_{0,n}$ of the n^{th} overtone, the electrode area A, and the shear modulus of quartz μ_q. For QCM measurements conducted in vacuum or gaseous environments, this equation in its simple form is very well suited for translating frequency shifts into mass changes, enabling the detection of mass variations on the order of a few nanograms. However, in order to provide insights relevant for electrochemical measurements, the QCM must be operable in an electrolyte solution and therefore capable of performing measurements in contact with a liquid medium. This presents a challenge because the resonance frequency generally depends on multiple factors. When the sensor is immersed in a liquid medium such as water, the oscillation of the crystal couples to the surrounding medium, leading to damping of the oscillation. This damping is also reflected as a shift in the resonance frequency [80]. The extent of the damping strongly depends on the density and viscosity of the medium, meaning that these parameters can also significantly influence the sensor's resonance frequency [81].

To reliably interpret resonance frequency changes in liquid environments, it is therefore necessary to also quantify the damping of the oscillation caused

by the medium. Damping of the oscillation corresponds to an energy loss to the surrounding medium, making the quantification of dissipated energy an excellent descriptor. The most widely used method for determining the dissipation D is based on measuring the decay time τ of an induced oscillation after switching off the driving power [82]:

$$D = \frac{1}{\pi f \tau} \tag{4.4}$$

where τ is defined as the time required for the oscillation amplitude to decay to $1/e$ of its initial value, where e is Euler's number. The stronger the damping of the oscillation, the higher the dissipation, which in turn allows conclusions to be drawn about the viscoelastic properties of the medium. Thus, for measurements in liquid media, both Δf and ΔD are typically monitored simultaneously, facilitating a more reliable interpretation of the observed resonance frequency changes [83]. If during a frequency shift the dissipation remains unchanged, the Sauerbrey equation provides a very good approximation even in liquid environments and can be used to determine mass changes. If, however, the dissipation changes, a purely gravimetric interpretation of the frequency shift is no longer valid. Instead, changes in dissipation indicate variations in viscoelastic properties or morphology at the crystal surface [83, 84]. Monitoring the dissipation thus yields additional information about the properties of deposited surface layers and can, for example, be employed for the characterization of polymer films.

When combined with electrochemical measurements, the technique is then called electrochemical quartz crystal microbalance with dissipation monitoring (EQCM-D). To enable the simultaneous use of both characterization methods, one of the electrodes on the quartz sensor must simultaneously also function as the WE in a three-electrode setup. This, in turn, requires that only this electrode is in contact with the electrolyte solution. To facilitate such measurements, the dip holder schematically shown in Figure 4.3 was employed in the studies in Paper I. In this configuration, the quartz crystal is mounted such that only the top electrode is exposed to the surrounding environment, while the bottom electrode is positioned inside the holder and thus shielded from contact with any external media. This arrangement allows the top electrode to serve as the WE, enabling electrochemical measurements such as CV to be performed, while simultaneously recording changes in resonance frequency and dissipation. Although the electrodes on quartz sensors used for QCM measurements are typically made of gold, the material of the top electrode in an EQCM-D setup is, in principle, freely selectable. Therefore, quartz sensors with top electrodes made of platinum, carbon, and gold were investigated in the experiments presented in Paper I.

4.1.1.2 Rotating Disk Electrode (RDE)

Another powerful tool for electrochemical measurements is the rotating disk electrode (RDE). This method is among the most widely used analytical tools, particularly in the field of catalysis research. The experimental arrangement

differs only slightly from a conventional three-electrode setup. The key difference lies in the design of the WE, which consists of a disk electrode, typically made of glassy carbon (GC), embedded in an insulating, chemically resistant polymer housing. This assembly is mounted onto an electric motor, allowing the electrode to rotate during electrochemical measurements. Rotation of the electrode in the liquid electrolyte induces convection, enabling a continuous and well-controlled exchange of the solution in the vicinity of the electrode surface. This is especially important when investigating reactions with fast kinetics or involving gaseous reactants with low solubility, as such reactions are otherwise easily limited by mass transport via diffusion and migration. The RDE thus provides a straightforward and effective means of controlling the mass transport of reactants to the WE [16].

When catalyst material is deposited onto the GC disk and investigated in such a setup, the well-defined mass-transport conditions allow for the extraction of information about the kinetic properties of the system [16]. By applying appropriate measurement protocols, important kinetic parameters such as the kinetic current density and, subsequently, the exchange current density can be determined [16, 85]. It is precisely this possibility that makes the use of a RDE so valuable for evaluating catalyst performance, and it is therefore used as standard for evaluating FC catalysts for both HOR and ORR.

Within the scope of this thesis, RDE measurements were primarily used in Paper II. In addition to the extraction of kinetic parameters in the studies presented in Paper II, RDE measurements were also employed in combination with degradation investigations using accelerated stress tests (ASTs). An AST refers to an electrochemical measurement protocol designed to simulate the ageing of an electrode. The effects of such ASTs can be identified from electrochemical data. To determine the underlying causes and mechanisms leading to degradation, it is, however, often necessary to examine the fine structure of the electrode. This requires a simultaneous evaluation using imaging methods as, for example, identical location transmission electron microscopy (IL-TEM), which will be discussed in more detail in the following sections. At this point, the focus is instead on how the corresponding samples can be measured within an RDE setup.

In order to combine RDE and IL-TEM, the samples must be on a specific substrate structure commonly used in electron microscopy. For this purpose, so-called TEM grids are loaded with the catalyst material, for example CL material. Those grids are small, highly delicate gold meshes with a very low thickness of only a few hundred micrometers. To enable measurements of these grids within a three-electrode setup, they must be fixed onto the WE in order to guarantee electrical contact during electrochemical measurements. Subsequently, however, they must also be removable again for further analysis. For the studies in Paper II, a cap as shown in Figure 4.4a was used to fix the samples in place. This cap is mounted onto the RDE head. The cap features several pins that secure the sample on the surface of the GC disk once the cap is firmly seated on the RDE head. At the same time, the cap is designed to be sufficiently open so that access of the electrolyte solution to the electrode is disturbed as little as possible. This design allows the RDE to be

rotated at arbitrary speeds during the measurement while maintaining electrical contact with the grid. The overall setup of this combined RDE measurement configuration is shown in Figure 4.4b.

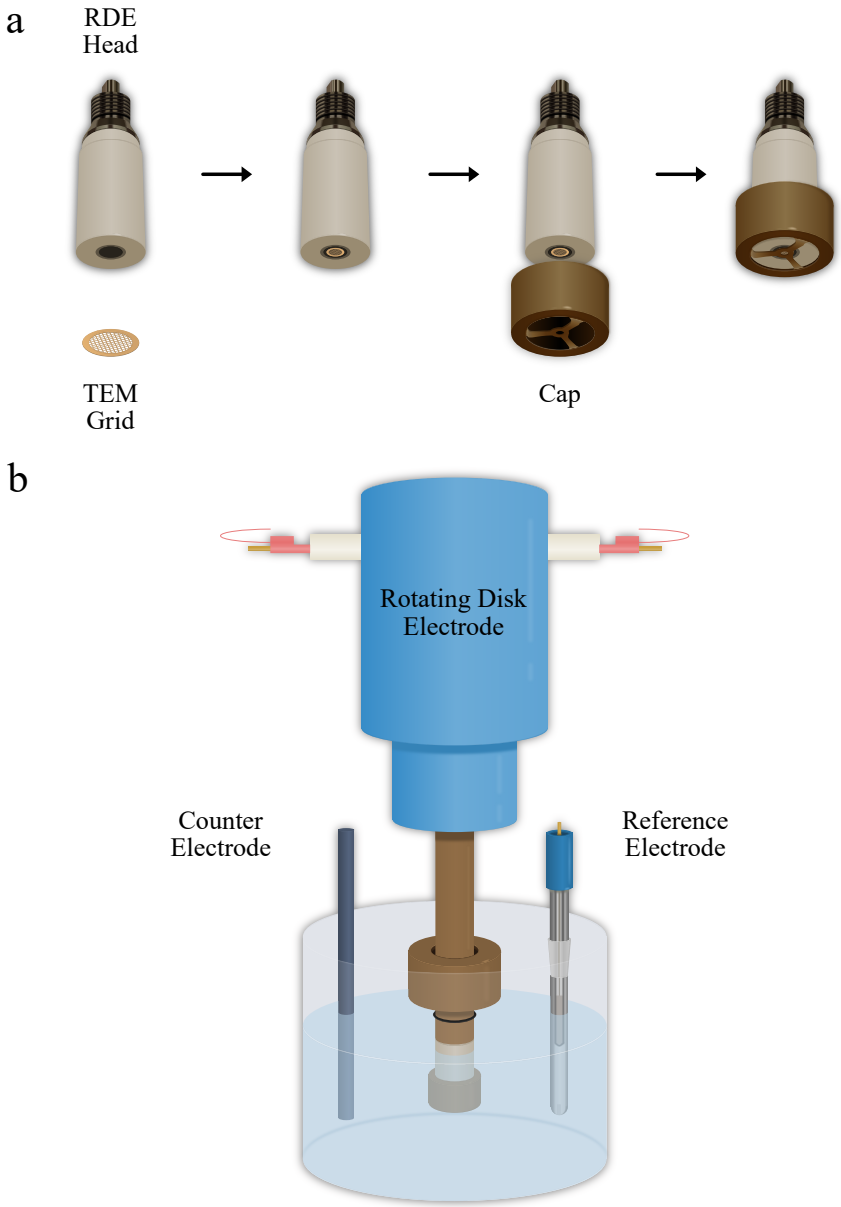

Figure 4.4: Schematic illustration of the experimental setup for IL-TEM measurements in combination with RDE measurements. a) shows the modified RDE head assembly process. b) shows the setup in a three-electrode cell.

4.2 Physical Characterization

In addition to electrochemical characterization, the studies in this thesis also included physical characterization. This is typically performed ex-situ and aims to analyze the structural properties of the samples. For this purpose, high-resolution, imaging-based characterization techniques such as electron microscopy are particularly well suited.

4.2.1 Electron Microscopy

Electron microscopy is a subclass of microscopy techniques and therefore refers to a set of instruments used for imaging objects at very high magnification. The concept of microscopy has been known for several centuries now and was initially developed using optical light microscopes. However, when using light in the visible range as the illumination source, significant limitations arise when attempting to image samples with structures only a few nanometers in size. This limitation was predicted by Ernst Abbe and is primarily based on the dependence of optical resolution on the wavelength of illumination [86], as expressed by the following equation:

$$d = \frac{\lambda}{2n\sin(\alpha)} \tag{4.5}$$

where d is the smallest resolvable distance between two imaged objects, λ the wavelength, n the refractive index, and α the aperture angle. Since the shortest wavelength of visible light is approximately 400 nm in the blue region, conventional optical microscopy methods cannot resolve structures smaller than about 100 nm. To overcome this resolution limit, microscopy using electrons instead of visible light as the source of illumination was developed. Because electrons exhibit both particle and wave characteristics, they can be assigned a specific wavelength, the so-called de Broglie wavelength, which depends on the kinetic energy of the electrons. When electrons are accelerated by an electric field with a given accelerating voltage V, their wavelength is given by [87]:

$$\lambda = \frac{hc}{\sqrt{eV(2m_0c^2 + eV)}} \tag{4.6}$$

where h is Planck's constant, c the speed of light, m_0 the electron rest mass, and e the electron charge. With sufficiently high accelerating voltages in the range of several hundred kilovolts, the theoretical resolution limit is reduced to only a few picometers. Although this limit cannot be achieved in practice due to lens aberrations, the resolution of electron microscopes is more than sufficient to image the structure of FC electrodes, as the size of catalyst particles typically lies within the nanometer range.

There exist two different approaches to the design and operating principle of an electron microscope, each based on slightly different concepts. The first subclass of electron microscopes is called the scanning electron microscope (SEM), and its working principle is reflected in the name. In this technique, an electron beam is manipulated by electromagnetic lenses so that it is focused

onto a very small area of the specimen. The focused beam then scans across the specimen in a raster pattern. Wherever the electron beam strikes the specimen, the electrons of the primary beam interact with the material primarily by knocking electrons out of the atomic shells of the atoms in the specimen, which generates secondary electrons. This interaction generates a variety of signals that can be detected, providing highly localized, high-resolution information about the specimen. The most commonly used signal is produced by detection of these secondary electrons, which have been knocked out of the electron shell by the primary beam. As these electrons have in general relatively low energy, they can only escape the specimen and be detected if they are generated close to the surface. This surface sensitivity therefore provides information about the specimen's topography. Thus, by scanning the primary electron beam and detecting secondary electrons, a pixel-by-pixel topographical image of the specimen can be created, typically resolving structures down to about 10 nm. In addition to secondary electrons, a SEM can detect other useful signals, such as characteristic X-rays, which is also called energy-dispersive X-ray spectroscopy (EDX). However, as these signals were not employed in the studies presented in this thesis, they will not be discussed here in detail.

The second subclass of electron microscopes describes the transmission electron microscope (TEM). This type is based on the same working principles as optical light microscopes. Here, the wave nature of electrons plays a decisive role, and the image of the specimen is formed through the interaction of an electron wave with the specimen followed by magnification via a electromagnetic lens system with the following optical configuration: condenser lenses and apertures are used to shape an electron beam that is as parallel and coherent as possible, which then is used to illuminate the specimen. For the interaction of the electron wave with the specimen, the electrons must be transmitted through the specimen and subsequently imaged by an objective lens. The image plane of the objective lens is then projected onto the imaging system, such as a camera, using projector lenses. To enable electron transmission through the specimen, it must be prepared to be sufficiently thin, typically with thicknesses not exceeding approximately 100 nm. Since a TEM operates on the same principles as optical light microscopes, the resolution limit described in equation 4.5 can be applied here, allowing structures of only a few Ångström to be visualized. This type of electron microscope is therefore highly suitable for characterizing the size, shape, and even crystal structure of the catalyst NPs used in FCs, making it a widely employed tool for the physical characterization of CLs. Furthermore, the ability to combine this technique with additional signal detection methods, such as EDX, further enhances its significance for comprehensive material analysis.

Identical Location Transmission Electron Microscopy (IL-TEM)

In the field of heterogeneous catalysis research, the progressive tracking and monitoring of the same specimen region is of particular interest for identifying structural changes. For this purpose, an identical location on a specimen can be repeatedly imaged in a TEM, with the specimen typically subjected to

specific procedures between imaging steps that induce ageing, so-called ASTs. By comparing the different images at different stages of ageing, mechanisms responsible for the degradation of the system under investigation can be identified. The identical location transmission electron microscopy (IL-TEM) method has therefore become established in recent years for studying the degradation of FC electrode components [88]. Using IL-TEM studies, it was possible to observe the previously introduced degradation mechanisms of catalyst NPs, namely Ostwald ripening and particle coalescence, as well as detachment or dissolution [89–91]. It has also been shown that by adjusting the AST protocols, conditions can be identified that promote either corrosion of the catalyst or carbon support [63, 92]. In this context, IL-TEM can be combined with either half-cell experiments, as described in Chapter 4.1, or with experiments involving single-cell FCs. Identifying degradation mechanisms enables the development of strategies to mitigate them, and, in the same way, IL-TEM imaging plays a crucial role in verifying the effectiveness of such mitigation strategies. Accordingly, IL-TEM investigations were employed in Paper II for the development of mitigation strategies for catalyst degradation in AEMFC CLs.

4.3 Sample Preparation

In the studies presented in this thesis, model systems were employed to investigate processes that also occur in real FC systems. For this purpose, quartz crystals with electrodes made of CL materials were fabricated in Paper I and subsequently coated with a thin layer of ionomer. The electrodes composed of different materials were produced using physical vapor deposition (PVD). Additionally, quartz crystals with carbon electrodes were covered with a PEMFC CL by spray-coating. For the IL-TEM experiments described in Paper II, TEM samples with AEMFC CL were prepared by dip-coating in catalyst ink.

4.3.1 Physical Vapor Deposition (PVD)

PVD was primarily used to deposit electrodes onto quartz crystals, which were subsequently employed during EQCM-D measurements. One major advantage of PVD is the wide range of materials that can be evaporated and deposited. The process used for sample preparation relies on heating a target material with an electron beam, and is therefore referred to as electron-beam PVD. Both the target and the sample are placed inside a vacuum chamber, where the target material vaporizes once its temperature becomes sufficiently high. The vaporized material then diffuses through the chamber and begins to condense on all solid surfaces, including the sample. Typically, a QCM system is employed to monitor and control the thickness of the deposited material film with such precision that even layers of only a few Ångströms can be produced. For the samples used in this work, films of 200 nm platinum, gold, and carbon were evaporated onto the crystals, each with an intermediate layer of 3 nm titanium to improve adhesion of the electrode to the quartz crystal. The specific electrode geometry was achieved by using a mask during the vaporization process.

4.3.2 Spray-Coating of PEMFC Catalyst Layers

To measure a PEMFC CL using the EQCM-D technique, the work presented in Paper I included a spray-coating process for sample preparation. A quartz crystal served as the substrate, which had previously been coated with a carbon electrode via PVD. This substrate was then sprayed with a catalytic ink using an automated spraying system. The ink consisted of a mixture of all CL components, namely carbon-supported platinum catalyst and ionomer, as well as a blend of solvents. Since a single spray cycle deposits only a very thin layer of material, the quartz crystals underwent two spraying cycles. After each cycle, an evaporation step was carried out to ensure complete removal of the solvents contained in the ink.

4.3.3 TEM-Grid Preparation

For the IL-TEM measurements presented in Paper II, the samples were prepared on TEM grids made of gold, which served as the substrate. In this case, a catalytic ink was applied using a dip-coating process. Therefore, TEM grids simply were immersed in the ink and subsequently dried.

Chapter 5

Results

This chapter discusses and summarizes the results presented in Papers I and II, with particular emphasis on the sections to which I made significant contributions.

5.1 Influence of Nafion on the Mass Response of Fuel Cell Materials Measured in EQCM-D

To fully understand the exact working principle of a FC catalyst layer under operating conditions, it is essential to examine the interactions between the individual components. However, since a FC typically represents a complex and closed system, investigating a single type of interaction during operation without significantly disturbing the system is extremely challenging. To still gain insights into possible interactions and processes, it is often necessary to resort to simplified model experiments. These model systems reduce complexity, allowing specific relationships to be studied in isolation.

This approach was also adopted in Paper I. Instead of analyzing the CL within a full PEMFC, individual materials and their combinations were tested separately in EQCM-D experiments. This technique enables simultaneous electrochemical measurements and monitoring of mass and viscosity changes of the investigated electrodes within a three-electrode setup. Similar approaches have previously been applied in studies examining, for example, the dissolution behavior of platinum electrodes in acidic and alkaline electrolytes [93, 94]. Other studies have demonstrated the catalytic influence of platinum NPs on carbon electrode corrosion using comparable methods [95]. In contrast, the focus of Paper I was on understanding the interaction between ionomer and the remaining components, particularly the catalyst material. For this purpose, the effect of a Nafion layer on the mass and viscoelastic response of platinum and carbon electrodes during potential cycling was investigated. Additional experiments were conducted with gold electrodes to compare the behavior of platinum with that of another noble metal. Measurements were performed in both H_2SO_4 and $HClO_4$ to elucidate the influence of the electrolyte on

the observed phenomena. Finally, the results were compared with EQCM-D measurements on a representative PEMFC CL that was spray-coated onto a quartz crystal.

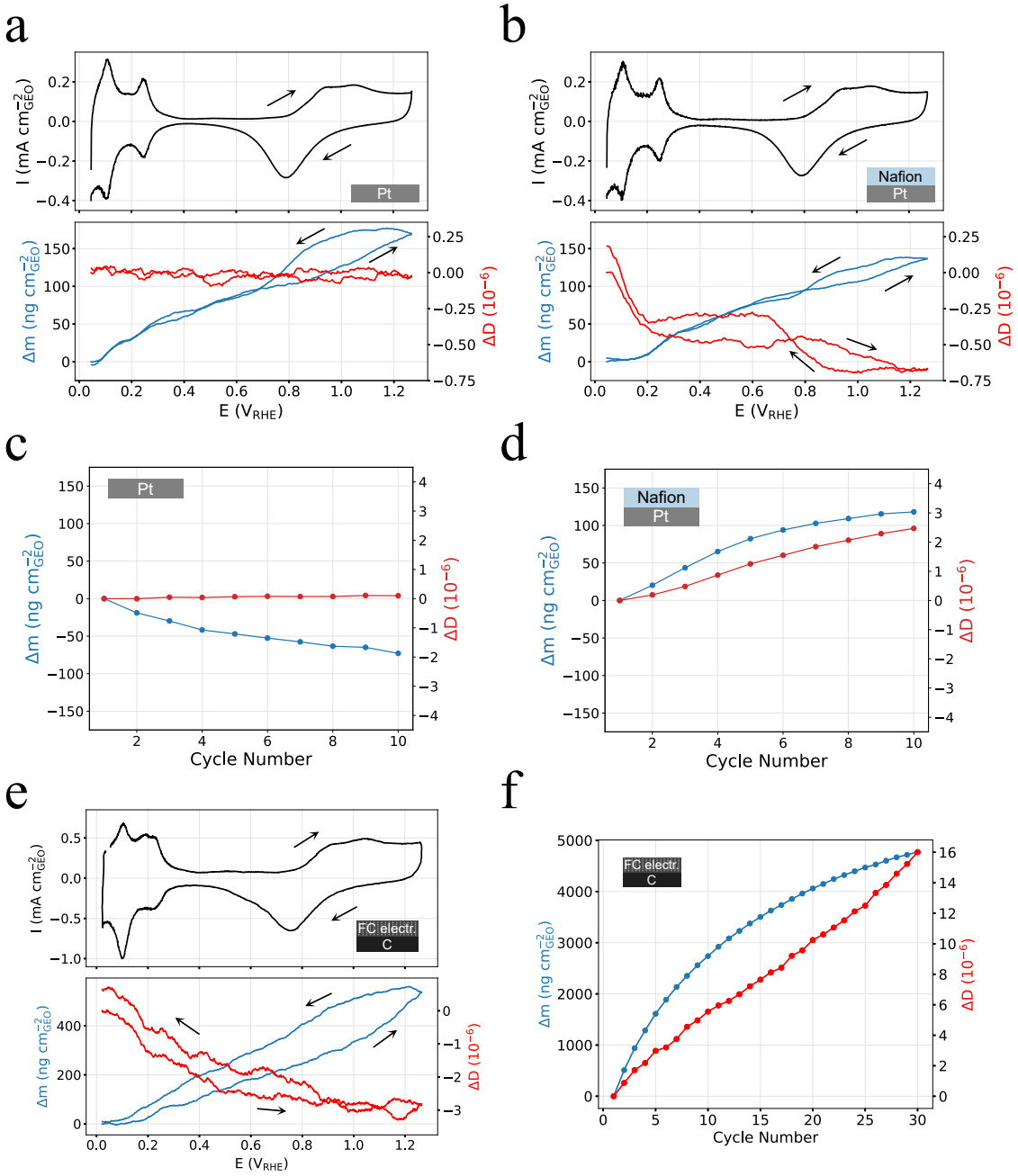

Figure 5.1: EQCM-D measurement data in 0.5 M H_2SO_4 for a) a platinum electrode without Nafion layer during one cycle of the CV, b) a platinum electrode with Nafion layer during one cycle of the CV, c) a platinum electrode without Nafion layer over 10 cycles of the CV, d) a platinum electrode with Nafion layer over 10 cycles of the CV, e) a spray-coated PEMFC CL electrode during one cycle of the CV, f) a spray-coated PEMFC CL electrode over 10 cycles of the CV. The CV data is plotted in black, the measured Sauerbrey-mass response in blue and the dissipation response in red, respectively.

In a direct comparison of EQCM-D measurements on platinum electrodes

without and with Nafion (Figure 5.1a and b), several noteworthy phenomena emerge that allow conclusions to be drawn regarding the interaction of the ionomer with the catalyst surface. In 0.5 M H_2SO_4, changes in the viscoelastic properties of the Nafion film can be observed in response to electrochemical changes of the catalyst surface. These changes occur predominantly during oxidation and reduction processes of the platinum electrode surface. Furthermore, the viscoelastic changes of the Nafion film are only partially reversible. Over multiple cycles of a CV, EQCM-D measurements reveal a pronounced increase in both the Sauerbrey mass change Δm and the dissipation ΔD (Figure 5.1d). For polymer systems, such behavior is typically interpreted as a substantial alteration of the viscoelastic properties due to water uptake into the polymer structure [83, 84, 96, 97]. This behavior differs markedly from that of a platinum electrode without Nafion (Figure 5.1c), where platinum dissolution is apparent over multiple CV cycles [94]. Comparable measurements performed on carbon and gold electrodes did not exhibit similar characteristics. It can therefore be assumed that the repeated oxidation and reduction of the platinum surface influences the Nafion film in such a way that additional water is driven into the polymer structure. As a consequence, the water content of the polymer film increases beyond its equilibrium state [98].

The precise origin of this effect cannot be conclusively determined based on the available measurement data. However, several plausible mechanisms can be proposed: First, it is well established that the functional groups of Nafion, namely the sulfonic acid groups, interact with the catalyst surface [99, 100]. It is therefore reasonable to assume that changes in the surface properties of the catalyst also affect the interaction between these functional groups and the surface. Secondly, the presence of an ionomer film on the electrode surface can give rise to an electrostatic barrier that impedes the migration of negatively charged ions from the electrolyte solution through the polymer. This barrier is described by the so-called Gibbs–Donnan effect [101, 102]. Thirdly, the oxidation of a platinum electrode in aqueous electrolyte proceeds via the consumption of water molecules. These water molecules may be drawn from the Nafion layer, leading to a stiffening of the polymer film due to the reduced water content. Conversely, during the reduction of an oxidized platinum surface, water is released and can be reabsorbed by the polymer layer, ultimately resulting in a decrease in film stiffness. Which of these effects predominantly governs the observed response of the Nafion film during CV cycling on a platinum electrode cannot be conclusively identified. However, EQCM-D measurements performed on the same electrode systems in 0.5 M $HClO_4$ indicate an additional influence of the electrolyte composition and, consequently, of the anions present in solution.

To assess the relevance of these findings with respect to practical PEMFC systems, additional EQCM-D measurements were conducted on a CL. For this purpose, a quartz sensor was coated with a CL as described previously. The measurements exhibit behavior very similar to that observed for Nafion-coated platinum electrodes. During oxidation and reduction processes, a modulation of the water content within the CL is observed (Figure 5.1e). In addition, over multiple CV cycles a pronounced, irreversible increase in Sauerbrey mass

and dissipation is detected (Figure 5.1f), indicating a significant,irreversible increase in the water content of the ionomer. These results suggest that the response during the measurement of a CL is dominated by interactions involving Nafion and the catalyst. Furthermore, they indicate that within a CL, the ionomer structure itself responds to the repeated oxidation and reduction of the catalyst NPs. These insights provide important contributions to the understanding of interactions between the various components of a PEMFC electrode and are highly relevant for the development of activation protocols aimed at conditioning electrodes and optimizing their performance [103].

5.2 Influence of TiO_2 on the Stability of Fuel Cell Catalysts Followed by IL-TEM

While some interactions between different materials within a FC electrode, such as those between the ionomer and the catalyst, directly affect FC performance, additional interactions among electrode components exert detrimental effects on performance over longer timescales. These include, in particular, processes that lead to electrode degradation and corrosion. Such phenomena often induce pronounced structural changes within the CL. Therefore, the investigation of degradation mechanisms using high-resolution imaging techniques has become a widely adopted approach. Methods such as IL-TEM, for example, enable the direct observation and tracking of degradation processes in FC electrodes. The insights gained from such studies further allow for the development of targeted strategies to mitigate electrode degradation.

This approach was employed in Paper II, which investigates the influence of a TiO_2 layer on the performance and stability of a AEMFC electrode. In this work, IL-TEM measurements of the electrode structure were combined with RDE measurements. Although additional experimental techniques were applied, the present discussion focuses exclusively on the RDE and IL-TEM degradation investigations, as these constitute my primary contribution to the study presented in Paper II.

In general, one of the major challenges limiting the performance of AEMFCs is the sluggish kinetics of the HOR compared to PEMFCs [66]. To enhance reaction kinetics, numerous approaches have been proposed, including the combination of palladium-based catalysts with metal oxides. Previous studies have demonstrated that adsorbed species can migrate between these two material phases, potentially resulting in a significant enhancement of reaction kinetics [68]. In addition, the stability of palladium-based AEMFC CLs has been reported to improve when combined with metal oxides [104]. Accordingly, in the studies presented in Paper II, AEMFC electrodes featuring palladium NPs supported on carbon were prepared using a thermal reduction method. Subsequently, TiO_2 was deposited onto the electrode structure by atomic layer deposition, ultimately forming a shell around the palladium NPs. Using RDE measurements, the kinetic parameters of electrodes with and without the TiO_2 protective layer were determined and systematically compared. In combination with IL-TEM, the effect of an AST was then investigated for both electrode

configurations, enabling a direct comparison of the corresponding degradation mechanisms.

Evaluation of RDE measurements for electrodes with and without a TiO_2 protective layer reveals pronounced differences in the reaction kinetics associated with the HOR. Evaluation of the kinetic parameters yields a more than threefold increase in the mass-specific exchange current density $j_{0,m}$, with a value of $98\,\mathrm{mA\,mg^{-1}}$ for the electrode featuring the TiO_2 protective layer, compared to $28\,\mathrm{mA\,mg^{-1}}$ for the uncoated electrode. Here, the mass refers to the palladium content in the electrode. After normalization to the respective ECSA, specific exchange current densities of $j_{0,s} = 0.193\,\mathrm{mA\,cm^{-2}}$ for the electrode with TiO_2 and $0.089\,\mathrm{mA\,cm^{-2}}$ for the electrode without an additional protective layer are obtained. These results demonstrate that palladium NPs supported on carbon and combined with a thin TiO_2 layer exhibit significantly enhanced catalytic activity toward the HOR in AEMFCs. The TiO_2 shell suppresses the formation of palladium hydride phases, a phenomenon in which adsorbed hydrogen is incorporated into the palladium lattice [105], while simultaneously providing surface sites for the adsorption of OH^- species, which play a crucial role in alkaline HOR kinetics.

Furthermore, IL-TEM degradation measurements reveal pronounced differences in electrode stability depending on the presence of a TiO_2 protective layer. The applied AST protocol induces accelerated electrode ageing via potential cycling in the RDE setup between 0 V to 4 V vs. RHE at a scan rate of $100\,\mathrm{mV\,s^{-1}}$ under an argon atmosphere. In each case, the electrodes were subjected to a total of 7000 cycles, with IL-TEM imaging performed initially, after 4000 cycles, and after 7000 cycles. For palladium-based electrodes without an additional TiO_2 layer, TEM images (Figure 5.2a) already reveal substantial structural changes after 4000 cycles. These changes primarily involve alterations in the shape and spatial distribution of the palladium NPs, including the formation of oversized particles due to agglomeration and coalescence. After 7000 cycles, some of these large particles disappear, presumably as a consequence of losing contact with the carbon support. The carbon support itself remains largely unchanged throughout the experiments, aside from isolated alterations attributable to mechanical stress. In contrast, palladium-based electrodes with an additional TiO_2 protective layer exhibit significantly less pronounced structural changes under AST conditions (Figure 5.2b). Although the formation of oversized NPs can still be observed in isolated cases, this typically becomes apparent only after 7000 cycles. Overall, the treated electrodes display markedly improved structural stability, with only minor changes in electrode morphology.

High-magnification TEM images further allow the identification of the mechanisms responsible for palladium NPs growth (Figure 5.2c). Processes such as particle dissolution and growth can be observed and assigned to established degradation pathways. These correspond to the mechanisms introduced in Chapter 3.3.2, namely Ostwald ripening, migration-induced particle coalescence, and gradual NP dissolution. Migration followed by coalescence is indicated by a red circle, Ostwald ripening by a blue circle, and dissolution or detachment by a yellow circle.

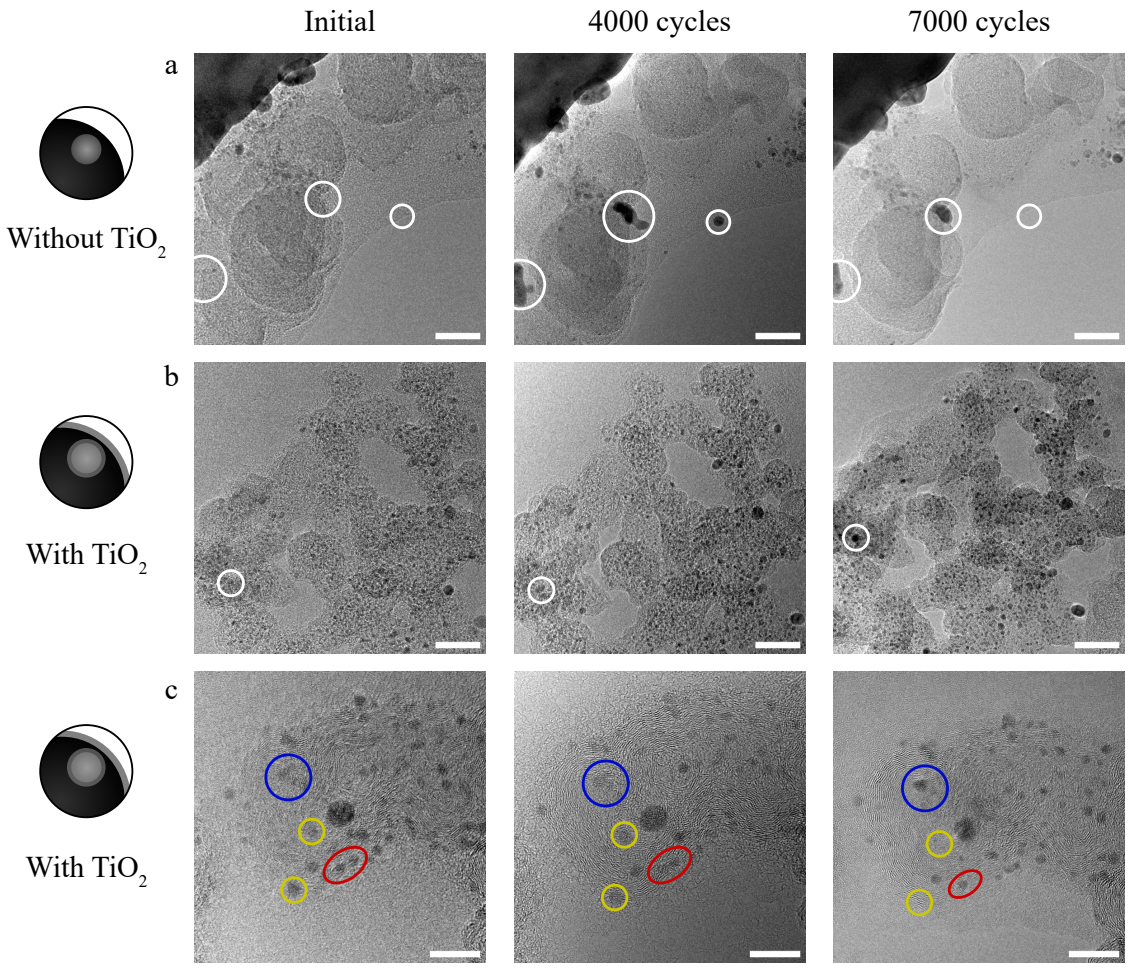

Figure 5.2: IL-TEM images of the initial electrode structure, after 4000 AST cycles, and after 7000 AST cycles. a) shows the structure of an electrode without TiO_2 protective layer. Important changes in the structure are marked in white. The scale bar corresponds to 30 nm. b) shows the structure of an electrode with TiO_2 protective layer. Important changes in the structure are marked in white. The scale bar corresponds to 30 nm. c) shows high-magnification images of the structure of an electrode with TiO_2 protective layer. Different degradation pathways for the NPs are marked in different colors, with migration followed by coalescence being marked in red, Ostwald ripening in blue, and dissolution or detachment in yellow. The scale bar corresponds to 10 nm.

Altogether, the IL-TEM studies presented in Paper II demonstrate a substantial improvement in the stability of palladium NPs as catalysts in AEMFC electrodes through the implementation of a TiO_2 shell structure. At the same time, enhanced catalytic activity resulting from the presence of the TiO_2 shell was observed. These effects are enabled by the suppression of palladium hydride phase formation and by the availability of adsorption sites for OH^- species on the TiO_2 shell structure.

Chapter 6

Conclusion & Outlook

In the context of ongoing climate change, it is of paramount importance to implement and further develop alternative systems for the generation, storage, and conversion of energy. Fuel cells (FCs) constitute a central component of hydrogen-based energy systems in particular, representing a crucial element for efficient conversion of chemically stored energy into electrical power. Among these, polymer-electrolyte-based FCs, such as proton exchange membrane fuel cells (PEMFCs) and anion exchange membrane fuel cells (AEMFCs), are especially promising candidates for the electrification of the transportation sector due to their low operating temperatures and comparatively straightforward handling. As such, they offer significant potential for the realization of a more sustainable energy system.

For the optimization of polymer-electrolyte-based FCs, a detailed understanding of the fundamental operating principles of these systems is essential. This thesis investigated the interactions between various electrode components in both PEMFCs and AEMFCs and assessed the impact of these interactions on FC performance. To this end, changes in electrode structure were identified and their underlying causes analyzed. In particular, the mutual influence of catalyst and ionomer within the electrode during operation was examined. Furthermore, the effect of applying a protective metal-oxide layer on catalytic activity and stability was systematically investigated.

Based on electrochemical quartz crystal microbalance with dissipation monitoring (EQCM-D) measurements, the interaction between Nafion and platinum during potential cycling was studied. It was observed that the polymer responds to changes in the oxidation state of the platinum surface with pronounced modulations in the polymer's water content. Especially during oxidation and reduction of the platinum electrode, clear changes in the viscoelastic properties of the Nafion film were detected, which can be attributed to variations in hydration. As these changes were only partially reversible, the Nafion film exhibited a cumulative increase in water content over successive potential cycles. This demonstrates that the ionomer within a PEMFC electrode undergoes structural reorganization in response to changes in the surface properties of platinum. These findings were corroborated by

EQCM-D investigations conducted on a PEMFC catalyst layer (CL), in which highly similar behavior was observed.

The influence of TiO_2 on the activity and stability of palladium nanoparticles (NPs) in a AEMFC electrode was investigated using a combination of rotating disk electrode (RDE) measurements and identical location transmission electron microscopy (IL-TEM) imaging. In the presence of TiO_2, an enhanced catalytic activity toward the alkaline hydrogen oxidation reaction (HOR) was observed, which can be attributed to improved adsorption properties for reactant species. In addition, a positive effect on catalyst stability was identified. Compared to electrodes without a protective layer, significantly reduced aggregation and coalescence of catalyst NPs were observed. On this basis, a viable mitigation strategy and an improved electrode architecture were proposed, which may contribute to enhanced AEMFC performance in future applications.

Although the studies conducted in this thesis provide valuable insights into the interactions between different components of polymer-electrolyte-based FCs, several limitations must be considered. For instance, EQCM-D measurements revealed clear changes in the viscoelastic properties and water content of the Nafion film during potential cycling, but the technique does not allow direct identification of the underlying structural or chemical modifications within the polymer. Resolving the details of the structural changes would require complementary analytical methods with molecular sensitivity, such as Raman or IR spectroscopy performed under comparable experimental conditions. Another important limitation arises from the model-system character of the experimental setups. Most measurements were carried out in liquid electrolytes and under simplified conditions that differ substantially from the operational environment of practical FCs. While such controlled systems enable the isolation of individual mechanisms, they cannot confirm whether the identified processes occur in the same way under realistic fuel cell operating conditions. Additional studies on real FCs or under more application-relevant conditions are therefore necessary to validate the transferability of the proposed mechanisms.

Despite these limitations, the results of this work open several promising avenues for future research. For instance, the pursuit of perfluorosulfonic acid (PFSA) free FCs necessitates the development of hydrocarbon-based alternatives. Although these alternatives often exhibit similar functional behavior, they differ markedly in their underlying chemistry. These differences are expected to lead to altered interactions between the ionomer and both catalyst and support materials. It would therefore be highly valuable to extend the EQCM-D investigations in this direction and to study the interactions of hydrocarbon-based ionomers with different catalyst materials. In addition, IL-TEM investigations offer substantial potential for the identification and differentiation of degradation mechanisms and should continue to be employed in future studies. On the one hand, this applies to controlled model experiments, for example within the RDE setup, to investigate the influence of metal-oxide layers on carbon support corrosion. On the other hand, the application of such techniques to measurements on realistic FC systems is equally important, as it increases the relevance of the findings for the operation of practical devices.

Overall, this thesis contributes to a deeper understanding of the complex

interactions between different materials within polymer-electrolyte-based FCs through the combined use of complementary experimental techniques. Together with continued research efforts, these insights have the potential to further advance the understanding of this promising technology and to facilitate its successful implementation within the future energy system of our society.

Acknowledgements

The work in this thesis was performed within the Competence Centre for Catalysis, which is hosted by the Chalmers University of Technology and financially supported by the Swedish Energy Agency and the member companies Johnson Matthey, Perstorp, PowerCell, Preem, Scania CV, Umicore and Volvo Group.

First and foremost, I would like to express my deepest gratitude to my supervisor, Björn Wickman, for giving me the opportunity to write this licentiate thesis. Under his guidance, I received unwavering support and insightful advice throughout this journey. I am also sincerely thankful to my examiner, Henrik Grönbeck, and my co-supervisor, Magnus Skoglundh, for their valuable input and for always taking the time to address questions and challenges related to my work.

I am truly grateful to all current and former members of the Division of Chemical Physics for creating such an inspiring and welcoming environment. Your curiosity and enthusiasm have made every discussion both enjoyable and enlightening. A special thanks goes to the Electrochemistry Group as working alongside you has been a privilege, and you have made this journey not only scientifically rewarding but also genuinely fun and memorable.

I would also like to thank my office mates, Linnéa, Isak, and Björn, for the countless conversations, shared laughs, and support during long days in the office. You turned the office into a place I looked forward to coming to every day, and I am so glad to have shared this time with you.

Beyond the lab, I am deeply grateful to all my friends - both the old ones who have supported me for years and the new ones I've had the joy of meeting along the way. Each of you has played a part in making this journey meaningful, whether through encouragement, laughter, or simply being there when I needed a break from research. Finally, my heartfelt thanks go to my family for their unconditional support. I could not have done this without all of you!

Bibliography

1. Gueydan, M. *World energy consumption 1800-2000: the results* en-GB. Mar. 2022. https://www.encyclopedie-energie.org/en/world-energy-consumption-1800-2000-results/ (2025) (cit. on p. 1).
2. *The world energy context* en. text. Publisher: IAEA. May 2014. http://www.iaea.org/publications/magazines/bulletin/15-5/world-energy-context (2025) (cit. on p. 1).
3. Ritchie, H., Rosado, P. & Roser, M. Energy Production and Consumption. en. *Our World in Data.* https://ourworldindata.org/energy-production-consumption (2025) (July 2020) (cit. on p. 1).
4. IEA. *Global Energy Review 2025* en. https://www.iea.org/reports/global-energy-review-2025 (Paris, 2025) (cit. on p. 1).
5. Khan, M. A., Khan, M. Z., Zaman, K. & Naz, L. Global estimates of energy consumption and greenhouse gas emissions. *Renewable and Sustainable Energy Reviews* **29,** 336–344 (2014) (cit. on p. 1).
6. Hansen, J. *et al.* Climate impact of increasing atmospheric carbon dioxide. *Science* **213,** 957–966 (1981) (cit. on p. 2).
7. Barton, J. P. & Infield, D. G. Energy storage and its use with intermittent renewable energy. *IEEE transactions on energy conversion* **19,** 441–448 (2004) (cit. on p. 2).
8. Huber, K. *Molecular spectra and molecular structure: IV. Constants of diatomic molecules* (Springer Science & Business Media, 2013) (cit. on p. 2).
9. *Energy density* en. Page Version ID: 1317675199. Oct. 2025. https://en.wikipedia.org/w/index.php?title=Energy_density&oldid=1317675199 (2025) (cit. on p. 2).
10. *EU Hydrogen Strategy under the EU Green Deal | European Hydrogen Observatory* en. https://observatory.clean-hydrogen.europa.eu/eu-policy/eu-hydrogen-strategy-under-eu-green-deal (2025) (cit. on p. 2).
11. Kleen, G. & Gibbons, W. *Heavy-Duty Fuel Cell System Cost – 2023* en-GB. Aug. 2024. https://www.hydrogen.energy.gov/docs/hydrogenprogramlibraries/pdfs/review24/24004-hd-fuel-cell-system-cost-2023.pdf (2025) (cit. on p. 3).

12. Efficiency, E. & (EERE), R. E. *Fuel Cell Technical Team Roadmap* tech. rep. (Energy Efficiency and Renewable Energy (EERE), Washington, DC (United States), June 2013). https://www.osti.gov/biblio/1220127 (cit. on p. 3).

13. Whittaker, E. *A history of the theories of aether and electricity: vol. I: the classical theories; vol. II: the modern theories, 1900-1926* (Courier Dover Publications, 1989) (cit. on p. 5).

14. Volta, A. XVII. On the electricity excited by the mere contact of conducting substances of different kinds. In a letter from Mr. Alexander Volta, FRS Professor of Natural Philosophy in the University of Pavia, to the Rt. Hon. Sir Joseph Banks, Bart. KBPR S. *Philosophical transactions of the Royal Society of London,* 403–431 (1800) (cit. on p. 5).

15. Turner, E. *Elements of Chemistry: Including the Actual State and Prevalent Doctrines of the Science* (Taylor, Walton, and sold, 1841) (cit. on pp. 5, 6).

16. Bard, A. J., Faulkner, L. R. & White, H. S. *Electrochemical methods: fundamentals and applications* (John Wiley & Sons, 2022) (cit. on pp. 6, 10, 11, 43).

17. Hamann, C. H., Hamnett, A. & Vielstich, W. *Electrochemistry* (Wiley-VCH, 2007) (cit. on pp. 8, 9).

18. Atkins, P. & Jones, L. *Chemical principles* (Macmillan, 2010) (cit. on p. 8).

19. Dickinson, E. J. & Hinds, G. The Butler-Volmer equation for polymer electrolyte membrane fuel cell (PEMFC) electrode kinetics: A critical discussion. *Journal of the electrochemical society* **166,** F221 (2019) (cit. on p. 11).

20. Chemistry (IUPAC), T. I. U. o. P. a. A. *IUPAC - standard hydrogen electrode (S05917)* en. https://goldbook.iupac.org/terms/view/S05917 (2025) (cit. on p. 12).

21. Chorkendorff, I. & Niemantsverdriet, J. W. *Concepts of modern catalysis and kinetics* (John Wiley & Sons, 2017) (cit. on pp. 12–14).

22. Roduner, E. Understanding catalysis. *Chemical Society Reviews* **43,** 8226–8239 (2014) (cit. on p. 13).

23. Sabatier, P. *La catalyse en chimie organique* (C. Béranger, 1920) (cit. on p. 15).

24. Medford, A. J. *et al.* From the Sabatier principle to a predictive theory of transition-metal heterogeneous catalysis. *Journal of Catalysis* **328,** 36–42 (2015) (cit. on p. 15).

25. Grove, W. R. LVI. On a new voltaic combination: To the editors of the Philosophical Magazine and Journal. *The London, Edinburgh, and Dublin Philosophical Magazine and Journal of Science* **13,** 430–431 (1838) (cit. on p. 19).

26. Nicholson, W. Account of the new electrical or galvanic apparatus of Sig. Alex. Volta, and experiments performed with the same. *Journal of natural philosophy, chemistry and the arts* **4,** 179–191 (1800) (cit. on p. 20).

27. Ritchie, H. Sector by sector: where do global greenhouse gas emissions come from? *Our World in Data.* https://ourworldindata.org/ghg-emissions-by-sector (2020) (cit. on p. 20).

28. Zu, C.-X. & Li, H. Thermodynamic analysis on energy densities of batteries. *Energy & Environmental Science* **4,** 2614–2624 (2011) (cit. on p. 20).

29. Liu, Y.-T., Liu, S., Li, G.-R. & Gao, X.-P. Strategy of enhancing the volumetric energy density for lithium–sulfur batteries. *Advanced Materials* **33,** 2003955 (2021) (cit. on p. 20).

30. Dicks, A. L. & Rand, D. A. *Fuel cell systems explained* (John Wiley & Sons, 2018) (cit. on pp. 21–26, 28–30).

31. Barbir, F. & Gomez, T. Efficiency and economics of proton exchange membrane (PEM) fuel cells. *international journal of hydrogen energy* **22,** 1027–1037 (1997) (cit. on p. 22).

32. Mekhilef, S., Saidur, R. & Safari, A. Comparative study of different fuel cell technologies. *Renewable and Sustainable Energy Reviews* **16,** 981–989 (2012) (cit. on p. 24).

33. Kirubakaran, A., Jain, S. & Nema, R. A review on fuel cell technologies and power electronic interface. *Renewable and sustainable energy reviews* **13,** 2430–2440 (2009) (cit. on p. 24).

34. Fuller, T. & Perry, M. A historical perspective of fuel-cell technology in the 20th Century. *Journal of the electrochemical society* **149,** S59–S67 (2002) (cit. on p. 24).

35. Das, G., Choi, J.-H., Nguyen, P. K. T., Kim, D.-J. & Yoon, Y. S. Anion exchange membranes for fuel cell application: a review. *Polymers* **14,** 1197 (2022) (cit. on p. 24).

36. Choudhury, A., Chandra, H & Arora, A. Application of solid oxide fuel cell technology for power generation—A review. *Renewable and Sustainable Energy Reviews* **20,** 430–442 (2013) (cit. on p. 24).

37. Peighambardoust, S. J., Rowshanzamir, S. & Amjadi, M. Review of the proton exchange membranes for fuel cell applications. *International journal of hydrogen energy* **35,** 9349–9384 (2010) (cit. on pp. 25–27).

38. Hamrock, S. J. & Yandrasits, M. A. Proton exchange membranes for fuel cell applications. *Journal of Macromolecular Science, Part C: Polymer Reviews* **46,** 219–244 (2006) (cit. on p. 25).

39. Agmon, N. The grotthuss mechanism. *Chemical Physics Letters* **244,** 456–462 (1995) (cit. on p. 26).

40. Grot, W. *Fluorinated ionomers* (William Andrew, 2011) (cit. on p. 26).

41. Kusoglu, A. & Weber, A. Z. New insights into perfluorinated sulfonic-acid ionomers. *Chemical reviews* **117,** 987–1104 (2017) (cit. on p. 27).

42. Brunn, H. *et al.* PFAS: forever chemicals—persistent, bioaccumulative and mobile. Reviewing the status and the need for their phase out and remediation of contaminated sites. *Environmental Sciences Europe* **35,** 1–50 (2023) (cit. on p. 27).

43. Sunderland, E. M. *et al.* A review of the pathways of human exposure to poly-and perfluoroalkyl substances (PFASs) and present understanding of health effects. *Journal of exposure science & environmental epidemiology* **29,** 131–147 (2019) (cit. on p. 27).

44. Merle, G., Wessling, M. & Nijmeijer, K. Anion exchange membranes for alkaline fuel cells: A review. *Journal of Membrane Science* **377,** 1–35 (2011) (cit. on pp. 27, 34).

45. Varcoe, J. R. *et al.* Anion-exchange membranes in electrochemical energy systems. *Energy & environmental science* **7,** 3135–3191 (2014) (cit. on pp. 27, 28, 36).

46. Dekel, D. R. Review of cell performance in anion exchange membrane fuel cells. *Journal of Power Sources* **375,** 158–169 (2018) (cit. on p. 28).

47. Mustain, W. E., Chatenet, M., Page, M. & Kim, Y. S. Durability challenges of anion exchange membrane fuel cells. *Energy & Environmental Science* **13,** 2805–2838 (2020) (cit. on pp. 28, 36).

48. Gasteiger, H. A., Kocha, S. S., Sompalli, B. & Wagner, F. T. Activity benchmarks and requirements for Pt, Pt-alloy, and non-Pt oxygen reduction catalysts for PEMFCs. *Applied Catalysis B: Environmental* **56,** 9–35 (2005) (cit. on pp. 28, 32).

49. Van Dao, D., Adilbish, G., Le, T. D., Lee, I.-H. & Yu, Y.-T. Triple phase boundary and power density enhancement in PEMFCs of a Pt/C electrode with double catalyst layers. *RSC advances* **9,** 15635–15641 (2019) (cit. on p. 29).

50. Zhao, J., Liu, H. & Li, X. Structure, property, and performance of catalyst layers in proton exchange membrane fuel cells. *Electrochemical Energy Reviews* **6,** 13 (2023) (cit. on pp. 29, 33, 34).

51. Olbrich, W., Kadyk, T, Sauter, U, Eikerling, M & Gostick, J. Structure and conductivity of ionomer in PEM fuel cell catalyst layers: a model-based analysis. *Scientific reports* **13,** 14127 (2023) (cit. on p. 29).

52. Woo, S. *et al.* Current understanding of catalyst/ionomer interfacial structure and phenomena affecting the oxygen reduction reaction in cathode catalyst layers of proton exchange membrane fuel cells. *Current Opinion in Electrochemistry* **21,** 289–296 (2020) (cit. on p. 30).

53. Kucernak, A. R. & Zalitis, C. General models for the electrochemical hydrogen oxidation and hydrogen evolution reactions: Theoretical derivation and experimental results under near mass-transport free conditions. *The Journal of Physical Chemistry C* **120,** 10721–10745 (2016) (cit. on p. 31).

54. Durst, J., Simon, C., Hasché, F. & Gasteiger, H. A. Hydrogen oxidation and evolution reaction kinetics on carbon supported Pt, Ir, Rh, and Pd electrocatalysts in acidic media. *Journal of The Electrochemical Society* **162,** F190 (2014) (cit. on p. 31).

55. Adzic, R. *Recent advances in the kinetics of oxygen reduction* tech. rep. (Brookhaven National Lab., Upton, NY (United States), July 1996). `https://www.osti.gov/biblio/259357` (cit. on p. 31).

56. Collier, A., Wang, H., Yuan, X. Z., Zhang, J. & Wilkinson, D. P. Degradation of polymer electrolyte membranes. *International Journal of Hydrogen Energy* **31,** 1838–1854 (2006) (cit. on pp. 32, 33).

57. Nørskov, J. K. *et al.* Origin of the overpotential for oxygen reduction at a fuel-cell cathode. *The Journal of Physical Chemistry B* **108,** 17886–17892 (2004) (cit. on pp. 32, 33).

58. Wang, J., Markovic, N. & Adzic, R. Kinetic analysis of oxygen reduction on Pt (111) in acid solutions: intrinsic kinetic parameters and anion adsorption effects. *The Journal of Physical Chemistry B* **108,** 4127–4133 (2004) (cit. on p. 32).

59. Min, M.-k., Cho, J., Cho, K. & Kim, H. Particle size and alloying effects of Pt-based alloy catalysts for fuel cell applications. *Electrochimica Acta* **45,** 4211–4217 (2000) (cit. on p. 32).

60. Yu, X. & Ye, S. Recent advances in activity and durability enhancement of Pt/C catalytic cathode in PEMFC: Part II: Degradation mechanism and durability enhancement of carbon supported platinum catalyst. *Journal of power sources* **172,** 145–154 (2007) (cit. on p. 33).

61. Topalov, A. A. *et al.* Towards a comprehensive understanding of platinum dissolution in acidic media. *Chemical Science* **5,** 631–638 (2014) (cit. on p. 34).

62. Roen, L., Paik, C. & Jarvi, T. Electrocatalytic corrosion of carbon support in PEMFC cathodes. *Electrochemical and solid-state letters* **7,** A19 (2003) (cit. on p. 34).

63. Strandberg, L., Shokhen, V., Skoglundh, M. & Wickman, B. Carbon support corrosion in PEMFCs followed by identical location electron microscopy. *ACS Catalysis* **14,** 8494–8504 (2024) (cit. on pp. 34, 47).

64. Bacon, F. Fuel cells, past, present and future. *Electrochimica Acta* **14,** 569–585. ISSN: 0013-4686. `https://www.sciencedirect.com/science/article/pii/0013468669870428` (1969) (cit. on p. 34).

65. Cong, Y., Yi, B. & Song, Y. Hydrogen oxidation reaction in alkaline media: From mechanism to recent electrocatalysts. *Nano Energy* **44,** 288–303 (2018) (cit. on p. 34).

66. Davydova, E. S., Mukerjee, S., Jaouen, F. & Dekel, D. R. Electrocatalysts for hydrogen oxidation reaction in alkaline electrolytes. *Acs Catalysis* **8,** 6665–6690 (2018) (cit. on pp. 35, 52).

67. Sheng, W. *et al.* Correlating hydrogen oxidation and evolution activity on platinum at different pH with measured hydrogen binding energy. *Nature communications* **6,** 5848 (2015) (cit. on p. 35).

68. Pagliaro, M. V. *et al.* Improving alkaline hydrogen oxidation activity of palladium through interactions with transition-metal oxides. *ACS Catalysis* **12,** 10894–10904 (2022) (cit. on pp. 35, 52).

69. Ge, X. *et al.* Oxygen reduction in alkaline media: from mechanisms to recent advances of catalysts. *Acs Catalysis* **5,** 4643–4667 (2015) (cit. on p. 35).

70. Sepa, D., Vojnovic, M. & Damjanovic, A. Kinetics and mechanism of O2 reduction at Pt in alkaline solutions. *Electrochimica Acta* **25,** 1491–1496 (1980) (cit. on p. 35).

71. Mao, X., Wang, L. & Li, Y. Understanding pH-dependent oxygen reduction reaction on metal alloy catalysts. *ACS Catalysis* **14,** 5429–5435 (2024) (cit. on p. 35).

72. Firouzjaie, H. A. & Mustain, W. E. *Catalytic advantages, challenges, and priorities in alkaline membrane fuel cells* 2019 (cit. on p. 35).

73. Miller, H. A. *et al.* Highly active nanostructured palladium-ceria electrocatalysts for the hydrogen oxidation reaction in alkaline medium. *Nano Energy* **33,** 293–305 (2017) (cit. on p. 36).

74. Rand, D. & Woods, R. A study of the dissolution of platinum, palladium, rhodium and gold electrodes in 1 M sulphuric acid by cyclic voltammetry. *Journal of Electroanalytical Chemistry and Interfacial Electrochemistry* **35,** 209–218 (1972) (cit. on p. 39).

75. Biegler, T, Rand, D. & Woods, R. Limiting oxygen coverage on platinized platinum; relevance to determination of real platinum area by hydrogen adsorption. *Journal of Electroanalytical Chemistry and Interfacial Electrochemistry* **29,** 269–277 (1971) (cit. on p. 40).

76. Trasatti, S & Petrii, O. Real surface area measurements in electrochemistry. *Pure and applied chemistry* **63,** 711–734 (1991) (cit. on p. 40).

77. Buttry, D. A. & Ward, M. D. Measurement of interfacial processes at electrode surfaces with the electrochemical quartz crystal microbalance. *Chemical Reviews* **92,** 1355–1379 (1992) (cit. on p. 40).

78. Kankare, J. Sauerbrey equation of quartz crystal microbalance in liquid medium. *Langmuir* **18,** 7092–7094 (2002) (cit. on p. 41).

79. Sauerbrey, G. Verwendung von Schwingquarzen zur Wägung dünner Schichten und zur Mikrowägung. *Zeitschrift für physik* **155,** 206–222 (1959) (cit. on p. 41).

80. Kanazawa, K. K. & Gordon II, J. G. The oscillation frequency of a quartz resonator in contact with liquid. *Analytica Chimica Acta* **175,** 99–105 (1985) (cit. on p. 41).

81. Kanazawa, K. K. & Gordon, J. G. Frequency of a quartz microbalance in contact with liquid. *Analytical Chemistry* **57,** 1770–1771 (1985) (cit. on p. 41).

82. Rodahl, M., Höök, F., Krozer, A., Brzezinski, P. & Kasemo, B. Quartz crystal microbalance setup for frequency and Q-factor measurements in gaseous and liquid environments. *Review of Scientific Instruments* **66,** 3924–3930 (1995) (cit. on p. 42).

83. Rodahl, M. *et al.* Simultaneous frequency and dissipation factor QCM measurements of biomolecular adsorption and cell adhesion. *Faraday discussions* **107,** 229–246 (1997) (cit. on pp. 42, 51).

84. Lucklum, R., Behling, C. & Hauptmann, P. Role of mass accumulation and viscoelastic film properties for the response of acoustic-wave-based chemical sensors. *Analytical Chemistry* **71,** 2488–2496 (1999) (cit. on pp. 42, 51).

85. Khadke, P. *et al.* A simple and effective method for the accurate extraction of kinetic parameters using differential Tafel plots. *Scientific reports* **11,** 8974 (2021) (cit. on p. 43).

86. Abbe, E. Beiträge zur Theorie des Mikroskops und der mikroskopischen Wahrnehmung. *Archiv für mikroskopische Anatomie* **9,** 413–468 (1873) (cit. on p. 45).

87. Kirkland, E. J. *Advanced computing in electron microscopy* (Springer, 1998) (cit. on p. 45).

88. Smykala, S., Liszka, B., Tomiczek, A. E. & Pawlyta, M. Using the IL-TEM Technique to Understand the Mechanism and Improve the Durability of Platinum Cathode Catalysts for Proton-Exchange Membrane Fuel Cells. *Materials* **17,** 1384 (2024) (cit. on p. 47).

89. Hodnik, N. & Cherevko, S. Spot the difference at the nanoscale: identical location electron microscopy in electrocatalysis. *Current opinion in electrochemistry* **15,** 73–82 (2019) (cit. on p. 47).

90. Lafforgue, C., Maillard, F., Martin, V., Dubau, L. & Chatenet, M. Degradation of carbon-supported platinum-group-metal electrocatalysts in alkaline media studied by in situ Fourier transform infrared spectroscopy and identical-location transmission electron microscopy. *ACS catalysis* **9,** 5613–5622 (2019) (cit. on p. 47).

91. Zadick, A., Dubau, L., Demirci, U. B. & Chatenet, M. Effects of Pd nanoparticle size and solution reducer strength on Pd/C electrocatalyst stability in alkaline electrolyte. *Journal of The Electrochemical Society* **163,** F781 (2016) (cit. on p. 47).

92. Shokhen, V., Strandberg, L., Skoglundh, M. & Wickman, B. Impact of accelerated stress tests on the cathodic catalytic layer in a proton exchange membrane (PEM) fuel cell studied by identical location scanning electron microscopy. *ACS Applied Energy Materials* **5,** 11200–11212 (2022) (cit. on p. 47).

93. Jerkiewicz, G., Vatankhah, G., Lessard, J., Soriaga, M. P. & Park, Y.-S. Surface-oxide growth at platinum electrodes in aqueous H2SO4: Reexamination of its mechanism through combined cyclic-voltammetry, electrochemical quartz-crystal nanobalance, and Auger electron spectroscopy measurements. *Electrochimica Acta* **49,** 1451–1459 (2004) (cit. on p. 49).

94. Strandberg, L. *et al.* Comparison of oxygen adsorption and platinum dissolution in acid and alkaline solutions using electrochemical quartz crystal microbalance. *ChemElectroChem* **9,** e202200591 (2022) (cit. on pp. 49, 51).

95. Wickman, B., Grönbeck, H., Hanarp, P. & Kasemo, B. Corrosion induced degradation of Pt/C model electrodes measured with electrochemical quartz crystal microbalance. *Journal of The Electrochemical Society* **157,** B592 (2010) (cit. on p. 49).

96. Zhang, G. & Wu, C. Quartz crystal microbalance studies on conformational change of polymer chains at interface. *Macromolecular rapid communications* **30,** 328–335 (2009) (cit. on p. 51).

97. Bandey, H., áRobert Hillman, A, Brown, M. & Martin, S. Viscoelastic characterization of electroactive polymer films at the electrode/solution interface. *Faraday Discussions* **107,** 105–121 (1997) (cit. on p. 51).

98. Höök, F. *et al.* Variations in coupled water, viscoelastic properties, and film thickness of a Mefp-1 protein film during adsorption and cross-linking: a quartz crystal microbalance with dissipation monitoring, ellipsometry, and surface plasmon resonance study. *Analytical chemistry* **73,** 5796–5804 (2001) (cit. on p. 51).

99. Masuda, T., Sonsudin, F., Singh, P. R., Naohara, H. & Uosaki, K. Potential-dependent adsorption and desorption of perfluorosulfonated ionomer on a platinum electrode surface probed by electrochemical quartz crystal microbalance and atomic force microscopy. *The Journal of Physical Chemistry C* **117,** 15704–15709 (2013) (cit. on p. 51).

100. Jiang, S. *et al.* Influence of the Pt/ionomer/water interface on the oxygen reduction reaction: insights into the micro-three-phase interface. *Chemical Science* **15,** 19290–19298 (2024) (cit. on p. 51).

101. Donnan, F. G. Theorie der Membrangleichgewichte und Membranpotentiale bei Vorhandensein von nicht dialysierenden Elektrolyten. Ein Beitrag zur physikalisch-chemischen Physiologie. *Zeitschrift für Elektrochemie und angewandte physikalische Chemie* **17,** 572–581 (1911) (cit. on p. 51).

102. Kimura, N. *et al.* Membrane potential across anion-exchange membranes in acidic solution system. *Journal of colloid and interface science* **286,** 288–293 (2005) (cit. on p. 51).

103. Van Der Linden, F., Pahon, E., Morando, S. & Bouquain, D. A review on the Proton-Exchange Membrane Fuel Cell break-in physical principles, activation procedures, and characterization methods. *Journal of Power Sources* **575,** 233168 (2023) (cit. on p. 52).

104. Douglin, J. C. *et al.* Elucidating the degradation mechanisms of Pt-free anode anion-exchange membrane fuel cells after durability testing. *Journal of Materials Chemistry A* **12,** 10435–10448 (2024) (cit. on p. 52).

105. Flanagan, T. B. & Lewis, F. Hydrogen absorption by palladium in aqueous solution. *Transactions of the Faraday Society* **55,** 1400–1408 (1959) (cit. on p. 53).